AFRL-RQ-WP-TR-2018-0099

AIRCRAFT GENERATOR DESIGN AND ANALYSIS

David Daniel Gross
Electrical and Computer Engineering
University of Dayton

SEPTEMBER 2018
Interim Report

AIR FORCE RESEARCH LABORATORY
AEROSPACE SYSTEMS DIRECTORATE
WRIGHT-PATTERSON AIR FORCE BASE, OH 45433-7542
AIR FORCE MATERIEL COMMAND
UNITED STATES AIR FORCE

NOTICE AND SIGNATURE PAGE

Using Government drawings, specifications, or other data included in this document for any purpose other than Government procurement does not in any way obligate the U.S. Government. The fact that the Government formulated or supplied the drawings, specifications, or other data does not license the holder or any other person or corporation; or convey any rights or permission to manufacture, use, or sell any patented invention that may relate to them.

Qualified requestors may obtain copies of this report from the Defense Technical Information Center (DTIC) (http://www.dtic.mil).

AFRL-RQ-WP-TR-2018-0099 has been reviewed and is approved for publication in accordance with assigned distribution statement.

This report is published in the interest of scientific and technical information exchange and its publication does not constitute the Government's approval or disapproval of its ideas or findings.

REPORT DOCUMENTATION PAGE

Form Approved
OMB No. 0704-0188

1. REPORT DATE *(DD-MM-YY)*	2. REPORT TYPE	3. DATES COVERED *(From - To)*
September 2018	Interim	15 September 2016 – 15 September 2018

4. TITLE AND SUBTITLE
AIRCRAFT GENERATOR DESIGN AND ANALYSIS

5a. CONTRACT NUMBER
In-house

5b. GRANT NUMBER

5c. PROGRAM ELEMENT NUMBER
62203F

6. AUTHOR(S)
David Daniel Gross

5d. PROJECT NUMBER
3145

5e. TASK NUMBER

5f. WORK UNIT NUMBER
Q1G2

7. PERFORMING ORGANIZATION NAME(S) AND ADDRESS(ES)
Electrical and Computer Engineering
University of Dayton
300 College Park
Dayton, OH 45469

8. PERFORMING ORGANIZATION REPORT NUMBER
AFRL-RQ-WP-TR-2018-0099

9. SPONSORING/MONITORING AGENCY NAME(S) AND ADDRESS(ES)
Air Force Research Laboratory
Aerospace Systems Directorate
Wright-Patterson Air Force Base, OH 45433-7542
Air Force Materiel Command
United States Air Force

10. SPONSORING/MONITORING AGENCY ACRONYM(S)
AFRL/RQQE

11. SPONSORING/MONITORING AGENCY REPORT NUMBER(S)
AFRL-RQ-WP-TR-2018-0099

12. DISTRIBUTION/AVAILABILITY STATEMENT
DISTRIBUTION STATEMENT A. Approved for public release. Distribution is unlimited.

13. SUPPLEMENTARY NOTES
PA Clearance Number: (Number) 88ABW-2018-2259; Clearance Date: 30 April 2018

14. ABSTRACT
Aerospace electrical power demands have been growing due to an increased amount of electrical load onboard aircraft. This increased load has come about as electrical power sources for various aircraft subsystems, such as pumps, compressors and flight controls, replace mechanical power sources. The main source of electrical power on an aircraft is a generator. The nature of emerging power demands on an aircraft causes increased temperatures and complex/dynamic loads; many contemporary generators are not necessarily designed to repeatedly tolerate such phenomena. Due to the need for high amounts of reliable electrical power among future aircraft, future generators should be designed for reliability, stability, power density and long-term durability. The objective of this thesis project was to determine if generator sizing techniques can be calculated to a reasonable accuracy for preliminary machine design optimization and analysis. A conceptual sizing tool was created in MATLAB using equations, assumptions, and rule-of-thumb metrics in an attempt to accomplish this objective. This work was performed through support of the AFRL/RQQ Intelligent Power Systems program.

15. SUBJECT TERMS
generator, power generation, electrical power generating system, aerospace power, generator design, wound-field synchronous

16. SECURITY CLASSIFICATION OF:			17. LIMITATION OF ABSTRACT:	18. NUMBER OF PAGES	19a. NAME OF RESPONSIBLE PERSON (Monitor)
a. REPORT	b. ABSTRACT	c. THIS PAGE			Chad N. Miller
Unclassified	Unclassified	Unclassified	SAR	82	19b. TELEPHONE NUMBER (Include Area Code) N/A

Aircraft Generator Design and Analysis

Undergraduate Honors Thesis – University of Dayton

David Daniel Gross
Department: Electrical and Computer Engineering

Advisor: Kevin Yost, M.S.
Air Force Research Laboratory – Wright-Patterson Air Force Base

May 2018

Abstract

Aerospace electrical power demands have been growing due to an increased amount of electrical load onboard aircraft. This increased load has come about as electrical power sources for various aircraft subsystems, such as pumps, compressors and flight controls, replace mechanical power sources. The main source of electrical power for an aircraft is a generator. The nature of emerging power demands on an aircraft causes increased temperatures and complex/dynamic loads; many contemporary generators are not necessarily designed to repeatedly tolerate such phenomena. Due to the need for high amounts of reliable electrical power among current and future aircraft, aerospace generators should be designed for reliability, stability, power density, and long-term durability. The objective of this thesis project was to determine if generator sizing techniques could be calculated to a reasonable accuracy for preliminary machine design optimization and analysis. A conceptual sizing tool was created in MATLAB using equations, assumptions, and rule-of-thumb metrics in an attempt to accomplish this objective. The tool was found to successfully analyze trends for given machine parameters, and provide initial sizing estimates for preliminary machine design. The confidence in the tool is strongest for the 40 kVA generator example simulated, due to the availability of similar generators (of which many aspects are known) for laboratory testing. Uncertainty increases in branching out from the 40 kVA generator design point, such as for the conceptual 250 kVA generator example simulated. Future work in this project includes improving weight/efficiency calculations and geometrical configurations, adding transient/subtransient reactance and thermal calculations, and using program results for Finite Element Analysis and direct-quadrature axis simulation programs.

Dedication

"For God and Country" (University of Dayton Motto)

AMDG ✚ JMJ

Acknowledgements

I would like to thank my advisor Kevin Yost, as well as Steven Iden, Benjamin Rhoads, and the Air Force Research Laboratory.

I would like to thank the University of Dayton point of contact, Dr. Guru Subramanyam, as well as Dr. Nancy Miller, Ramona Speranza, and the University of Dayton Honors Program.

I would like to thank my family and friends.

I would like to thank God, from whom comes all blessings.

Table of Contents

List of Tables

List of Figures

Chapter 1: Introduction

Aerospace Electrical Power Generating System (EPGS) requirements have been growing due to an increased demand of electrical power onboard aircraft. This demand is the result of a "more electric aircraft" (MEA), which has come about as electrical power sources for various aircraft subsystems, such as pumps, compressors, and flight controls, replace mechanical power sources [1], [2]. Figure 1 shows conventional aircraft power distribution, and Figure 2 shows MEA power distribution.

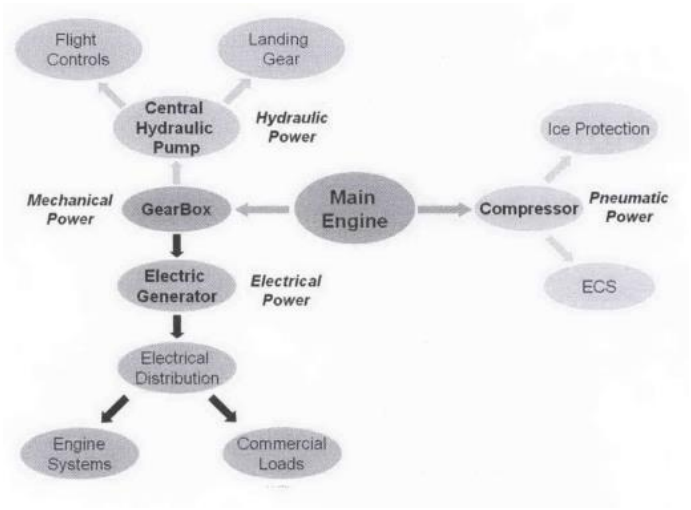

Figure 1: Schematic of conventional aircraft power distribution [2]

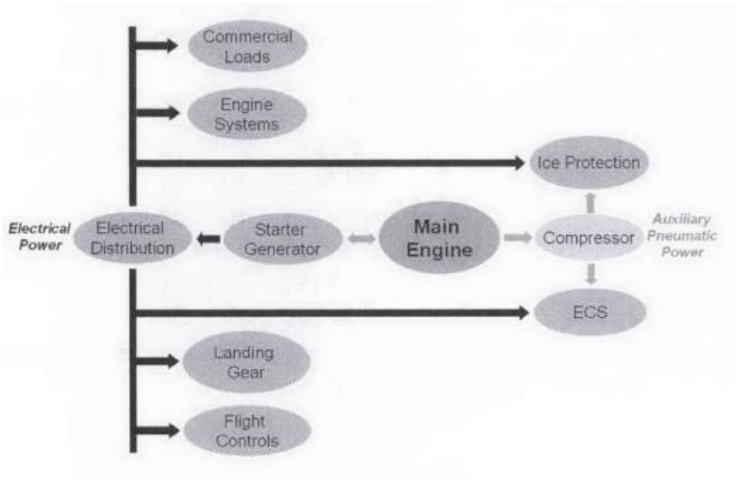

Figure 2: Schematic of MEA power distribution [2]

Figure 1 shows that many subsystems on an aircraft traditionally have had mechanical power sources that are extracted from an engine through geared mechanisms. For example, hydraulic power (used for flight controls and landing gear) in the past has come from mechanically sourced pumps that need to be continuously driven. The performance of mechanical sources for this example and other subsystems has been acceptable in the past [3]. The demand on mechanical sources by dynamic subsystem loads on the aircraft, however, is subservient to flight propulsion demands (since the mechanical power ultimately comes from the engine). This means that these auxiliary devices often operate outside of their ideal operating conditions, thus decreasing efficiency. An electrical power source associated with MEA, though it still has power losses, can be more efficient than traditional mechanical power onboard aircraft. Other benefits of MEA include: lower maintenance costs, fewer failures, and a reduction in weight that comes from hydraulic lines and fluid. [2]

The emergence of MEA, and the corresponding increased demand of reliable electrical power onboard aircraft, brings about the need for reliable electrical power sources. The main source of electrical power on an aircraft is a generator. A generator converts mechanical energy to electrical energy via applications of electromagnetics. The mechanical energy input for a generator comes from the engine in the form of a rotating shaft attached to the generator. Ideal properties of a generator are: robust (insensitive to factors causing unwanted variability), reliable, stable (both thermally and electrically), power dense, efficient, and adaptable (ability to operate in a variety of operating conditions) – properties which often yield contradictory design tradeoffs.

The electrical loads associated with MEA yield increased temperature and complex/dynamic load demands; many contemporary generators are not necessarily designed to repeatedly tolerate such phenomena. Because of the added stresses caused by these loads, the lifetimes of fielded generators are significantly reduced. Generator designs today often do not meet both the demands of MEA and a generator's ideal performance without significant tradeoff penalties [1]. Although tradeoffs exist, a goal is for their effects to be minimized. The objective of this thesis project is to determine if generator sizing techniques can be calculated to a reasonable accuracy for preliminary machine design optimization and analysis. Techniques for doing this include using equations, assumptions, and rule-of-thumb metrics.

This thesis project largely consists in designing a conceptual sizing tool (model) in MATLAB that will calculate generator sizing properties based off user inputs. The rest of the thesis is organized as follows: Chapter 2 presents the theory behind generators, with subsequent emphasis on aircraft generators. Chapter 3 discusses the sizing tool created for generator design and analysis. Finally, Chapter 4 consists of the conclusions and recommendations for future work.

Chapter 2: Theory

2.1: General

When a charge moves through a magnetic field, it experiences an electromagnetic force in the form of work. Consider that the charge is in a wire perpendicular to the lines of the magnetic field. As the charge moves through the wire, the force it experiences is along the wire, and the work done by the force per unit charge is voltage. [4]

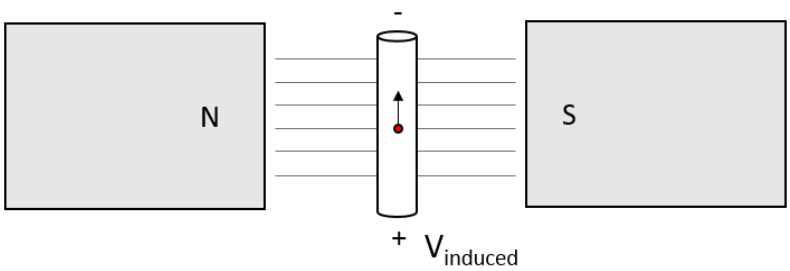

Figure 3: Charge moving through wire in magnetic field

Now consider that the wire is a rotating copper wire in a magnetic field (a simple generator). This field is caused by magnetic potential, or magnetomotive force (MMF). As the wire rotates in the field, voltages are induced in both sides of the wire. Since the sides are moving in opposite directions, the induced voltages are in series with one another and add. Due to the rotation of the wire, the magnitude of the induced AC voltage varies with time, taking a sinusoidal shape. [4]

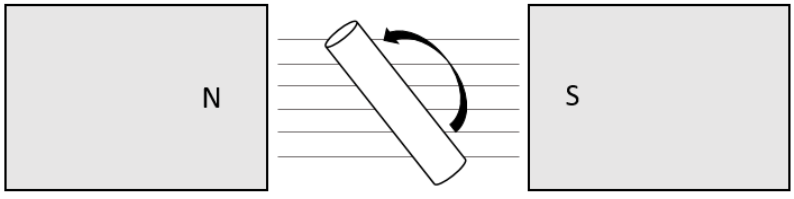

Figure 4: Rotating copper wire in magnetic field

A wire rotating through a magnetic field is not the only way voltage can be induced in the wire. All that is needed is a variation in the magnetic environment of the wire. This variation can come in different ways, including moving the wire in and out of the rotating field (such as by rotation of the wire), and changing the strength of the magnetic field (such as by rotation of the field). The voltage generated is known as electromotive force (EMF) and can be summarized by Faraday's Law [4]:

$$EMF = -N\frac{\Delta\Phi}{\Delta t} \quad (1)$$

$$EMF = electromotive\ force\ (voltage\ generated)$$
$$N = number\ of\ turns$$
$$\Phi = BA = magnetic\ flux$$
$$B = external\ magnetic\ field$$
$$A = area\ of\ coil$$
$$t = time$$

The purpose of the minus sign is to be inclusive of Lenz's Law, which accounts for a conservation of energy and states that the magnetic field of the induced current will oppose the initial change in magnetic flux through the wire. In addition, the EMF increases as the number of turns in the wire increases. Thus in practice it is beneficial for generators to have coils (multiple turns in a wire). As a coil rotates through a magnetic field (or as the magnetic field around the coil changes), the magnetic flux changes because the perpendicular area of the coil exposed to the magnetic field changes. So, according to Faraday's Law, the EMF is proportional to the change in magnetic flux with respect to time. For an AC generator, this change of flux is proportional to the rotational speed of the shaft. Thus as the shaft speed increases, so does the induced EMF. [4]

A generator converts mechanical energy to electrical energy, and consists of a rotor and a stator. The rotor is connected to the shaft, and spins within the stator. Because

either the coils can move or the magnetic field can move for voltage to be produced on the armature (the power-producing component of the generator), there are two options for how the coils and magnetic poles are placed within a generator:

- Magnetic poles are on the rotor and the armature is on the stator. Thus the field is rotating and the armature is stationary.

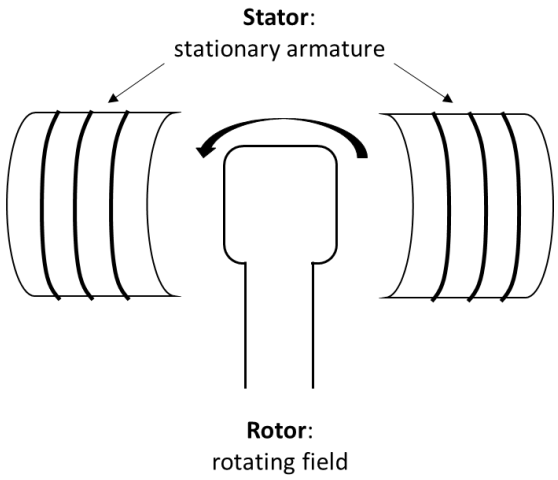

Figure 5: Rotating field and stationary armature

- Armature is on the rotor and the magnetic poles are on the stator. Thus the armature is rotating and the field is stationary. This layout is often called an inside-out configuration.

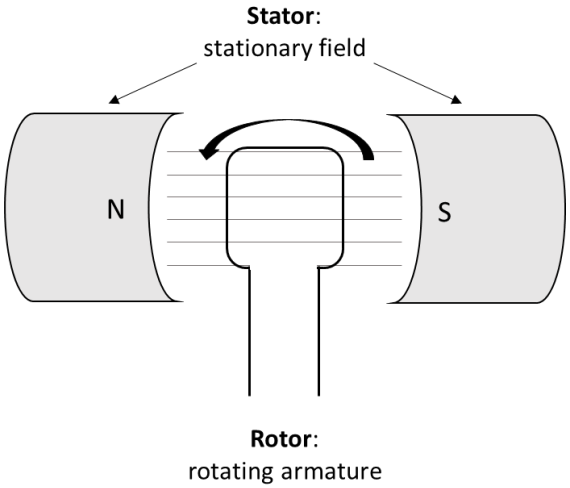

Figure 6: Stationary field and rotating armature

The magnetic field can either be produced by permanent magnets or electromagnets. Like electric circuits, there are also magnetic circuits; electric and magnetic circuits are analogous to one another. Table 1 and Figure 7 describe these analogies [5].

Table 1: Analogy of electric and magnetic circuits

	Electric Circuit	**Magnetic Circuit**
Driving Force	EMF (voltage: V)	MMF ($\mathcal{F}$)
Produces	Current ($I = V/R$)	Flux ($\Phi = \mathcal{F}/\mathcal{R}$)
Limited by	Resistance ($R = l/\sigma A$) (σ: conductivity; A: area)	Reluctance ($\mathcal{R} = l/\mu A$) (μ: permeability; A: area)

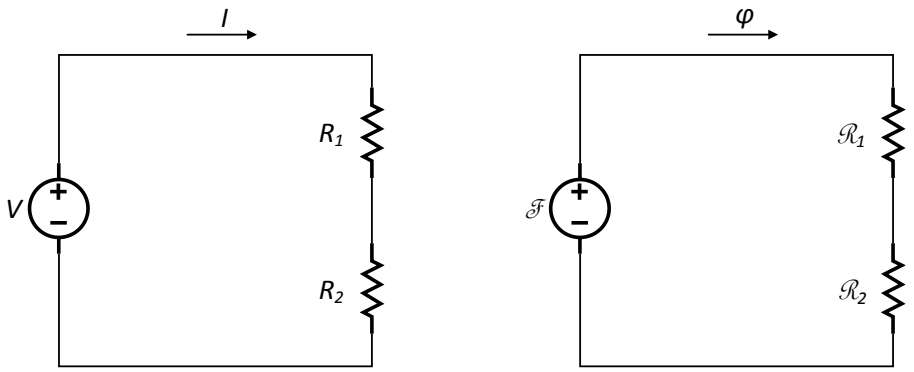

Figure 7: Analogy of electric (left) and magnetic (right) circuits

The generator equivalent circuit is seen in Figure 8. The current (I) arising out of the generated AC voltage (V_i, induced by field winding flux) experiences synchronous reactance (X_s) and resistance (R) before it reaches the terminals and outputs a terminal voltage (V_f).

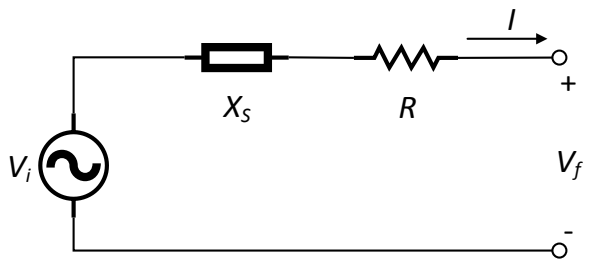

Figure 8: Generator equivalent circuit

The voltage at the terminals is given by Equation 2:

$$V_f = -RI - jX_sI + V_i \tag{2}$$

2.2: Aircraft Generator Considerations

There are many types of generators with various designs to suit their applications. As this thesis project is on aircraft generators, this section focuses on design aspects to consider for an aircraft generator.

2.2.1: Power and Voltage

The standard power equation consists of the following relationships [1]:

$$P\ \alpha\ \left(f_b, B_L, A, D^2, L_S, N_{rpm}\right) \tag{3}$$

$$P = power$$
$$f_b = form\ factor$$
$$B_L = magnetic\ loading$$
$$A = electrical\ loading$$
$$D = rotor\ diameter$$
$$L_S = stack\ length$$
$$N_{rpm} = shaft\ speed$$

The general output rms voltage equation (which is a form of Faraday's Law) is given by Equation 4 [6]:

$$E = \sqrt{2}\pi f_b N_\varphi f \Phi \quad (4)$$

$$E = rms\ voltage$$
$$f_b = form\ factor$$
$$N_\varphi = \#\ phase\ turns$$
$$f = frequency$$
$$\Phi = magnetic\ flux$$

Equation 4 is obtained by using the Fourier series representation equation of air gap magnetic flux density and the form factor, f_b, the penalty paid for good sinusoidal voltages. Doing so accounts for reduced rms voltage, because non-sinusoidal Fourier series effects and non-linearity will not yield pure sinusoidal waves. Thus replacing $\sqrt{2}\times\pi$ (approximately 4.44) with 4 is sometimes done if the multiplication factor to get ~4.44 is within f_b. In the thesis, the value of 4 is used in this way for the sizing tool.

2.2.2: Synchronous

Aircraft generators are synchronous machines. A synchronous machine can be described in the following manner [7]:

- A magnetic field is created on the rotor (assuming wound field – see Section 2.2.3).
- An external driving force (prime mover) is applied (i.e. the shaft is spun).
- Voltage is induced on the stator windings.
- "Synchronous" means that the output frequency is directly proportional to the shaft rotational speed (under steady-state conditions).

$$f = \frac{N_{rpm} p}{120} \quad (5)$$

$$f = frequency$$
$$N_{rpm} = shaft\ speed$$
$$p = \#\ poles$$

2.2.3: Wound Field

Aircraft generators are generally wound field machines. Wound field means that the magnetic field is produced by electromagnets, which consist of coils excited by DC power. The electromagnet is on the rotor. The MMF strength of the electromagnet is proportional to the current level flowing through the coil and the number of turns of the coil. As seen in Faraday's Law, the EMF is proportional to the rate of change of magnetic flux, which is proportional to the strength of the magnetic field. Thus, since the magnetic field strength can be adjusted, a benefit of wound field machines over permanent magnet machines is that the corresponding output voltage can be easily regulated, and quickly turned off if necessary. Disadvantages of using a wound field are that the machines with this design aspect can be complex due to the presence of an exciter machine (see Section 2.2.4), and weigh a substantial amount due to the large amount of coils. In addition, the large amount of coils limits rotational tip speed and causes winding losses, requiring extra cooling. The large benefit, however, of inherent voltage regulation for dynamic operations is important for aircraft electrical systems; thus wound field machines are preferred in aircraft. [8]

2.2.4: Multistage

Since aircraft generators are generally wound field, and the main electromagnet is on the rotor, DC excitation current must be provided on the rotor to the coils that form the electromagnet. In older generators, this excitation current for the main electromagnet was usually supplied by an exciter DC machine via slip rings mounted to the stator. In modern generators, however, the excitation current is typically supplied through a brushless excitation system. Thus, with such a system, it becomes appropriate to divide the

generator into two stages: the exciter stage (which provides the DC power for the main field electromagnet) and the main stage (the principal power-producing aspect of the machine). Figure 9 shows an aircraft generator schematic for such a generator, with corresponding pictures. The exciter stage (rotating field and stationary armature – inside-out configuration) is to the left of the vertical purple dashed line, and the main stage (stationary field and rotating armature) is to the right. A DC exciter field (electromagnet) is present on the stator, and AC voltage is induced on the armature of the exciter machine (present on the rotor) when the generator spins. The rectification system (diodes in Figure 9), present on the rotor, converts the AC power to DC, which flows through the coils of the main electromagnet and produces the main electromagnetic field. Now voltage can be induced on the main stage armature when the generator spins. [9]

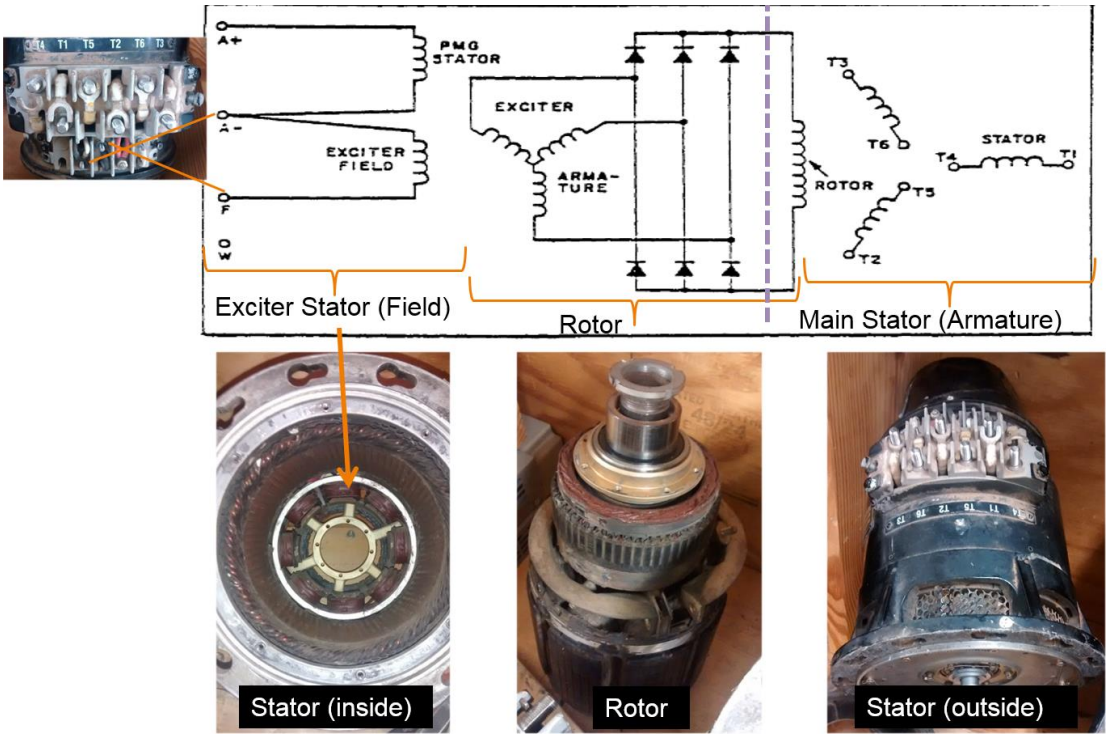

Figure 9: Generator schematic with corresponding pictures

Figure 10 shows a quartered generator of the type shown in Figure 9.

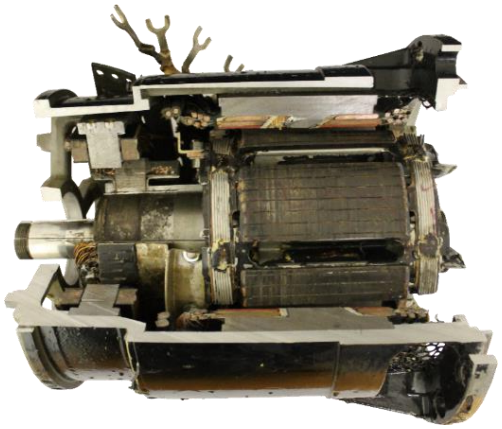

Figure 10: Quartered generator

A two-stage machine design eliminates the need for slip rings in providing power to the field, allowing for the only physical connection between the rotor and stator to be shaft bearings. However, with such a design, it can be difficult to measure the amp-turns on the main field when testing generators. In reality, there are three stages to the machine of the schematic shown in Figure 9, the third one being the permanent magnet (PMG) stator stage. The purpose of this stage is to provide the DC current needed by the exciter field. This stage, however, can be bypassed when testing by directly applying DC power to the field (this can be done without the need of slip rings since the exciter field is on the stator).

2.2.5: Stator Design

As mentioned earlier, the electromagnetic field source on aerospace wound field machines is on the rotor. So the armature windings are on the stator. Another important aspect of the stator is that, being made of steel, it helps direct the magnetic flux and completes the flux path for the magnetic circuit of the machine. There are slot-less and slotted design options for a stator. In a slot-less design, the armature coils are placed in the effective magnetic air gap. This option, however is not commonly used in

applications requiring wide operating conditions. Rather, slotted designs with steel teeth for the stator are typically used. A slotted design provides rigid housing for the coils and insulation, and the steel present in the teeth can help remove heat from the windings. A narrow air gap is also possible in a slotted design. A disadvantage, however, is the potential for cogging torque, which can cause vibrations – though this unwanted aspect can be reduced. Techniques for doing so include: using a fractional number of slots per pole per phase (see Section 2.2.12), skewing stator slots or poles, and adjusting the width of the stator slots. Skewing slots (or rotor poles) is the most effective means of reducing cogging torque [10], and the technique of skewing slots is discussed in Section 2.2.13. [8], [10]

2.2.6: Rotor Design

The rotor aspect ratio, defined as the length to diameter (L/D) ratio of the rotor, is an important factor in the performance of a machine. Typical aerospace designs have L/D ratios in the range of 0.3 to 2.0 [1]. A higher L/D ratio (longer length and smaller diameter) allows for lower inertia and faster mechanical response. Mechanical stresses at high speeds are lower, reducing end-turn conductor losses and allowing for a smaller shaft (which can have reduced friction losses and operate at higher speeds). A lower L/D ratio (shorter length and larger diameter) allows for a deeper stator slot depth, which provides more space for coil windings. This aspect decreases current density and allows for higher electrical loading. Too low of an L/D ratio, however, can cause the tip speed of the machine to exceed its maximum permissible tip speed (a copper winding balance limitation). This value is 650 ft/s (fps) for wound rotor machines [1]. [11]

2.2.7: Materials

Aircraft generators have copper windings (coils). The use of copper coils for electric machine windings has existed for many decades and is still universally common, largely due to copper's high conductivity, constancy over time, and low cost (in comparison to precious metals such as silver). Disadvantages, however, include significant losses at higher speeds/frequencies due to eddy current losses and skin effect (the tendency of high-frequency AC current to flow only on a conductor's outer layer). Aluminum has higher specific heat capacity and conductivity-to-mass ratio than copper. Aluminum also has a higher coefficient of thermal expansion (CTE) than copper, and so expands much more than copper at higher temperatures, yielding a lower volumetric density. Thus the use of aluminum coils in weight-sensitive applications can be beneficial, but skin effect and low volumetric density due to aluminum's CTE can be problematic. There has been recent research in the use of carbon nanotube (CNT) windings for electric machine applications. These windings have low mass density and no skin effect. But although CNT windings would be lightweight, they would take up a large amount of volume. [12]

The material used for the rotor and stator is magnetic steel. The purpose of the steel is to direct the magnetic flux throughout the machine. The type of steel chosen is based on various criteria, including: permeability, core (magnetic/iron) losses, saturation properties, and cost/availability. The four most common steel materials used are: low carbon, silicon, nickel alloy, and cobalt alloy. Due to their high cost, cobalt alloys are typically only used high performance situations, such as in aerospace and space applications. [8]

2.2.8: Torque Density

The torque density rating of a machine plays a large role in its physical sizing. A higher torque density design, or torque per rotor volume (TRV), yields a smaller rotor volume, while a lower TRV yields a larger rotor volume. Allowable torque density is largely determined by thermal aspects: the better a machine can be cooled, the higher the TRV and thus the smaller the volume. Since a goal of aerospace generators is to be power dense (i.e. have high power output for low volume), a higher TRV is generally desired. The torque density can be determined by air gap shear stress [13].

$$\sigma \propto AB \tag{6}$$

$$\sigma = shear\ stress$$
$$A = current\ density$$
$$B = flux\ density$$

$$\tau = \frac{T}{V_r} = \frac{\pi}{\sqrt{2}} k_w AB \tag{7}$$

$$\tau = torque\ density$$
$$T = torque$$
$$V_r = rotor\ volume$$

2.2.9: Air Gap

The air gap of a generator is the gap between, and physically separating, the rotor and the stator. A larger air gap allows for better voltage regulation and performance of the machine, but at the cost of power factor and efficiency. So a larger air gap allows more controllability in adjusting the voltage, and the generator can respond quickly since a high amount of energy is stored in the air gap [14]:

$$Stored\ Energy \approx \frac{B^2 \times Volume}{2\mu_o} \quad (8)$$

$$\mu_o = permeability\ of\ air$$
$$B = flux\ density$$

A narrow air gap, however, increases permeance (the ability of magnetic flux to flow through a material – inverse of reluctance) and minimizes flux leakage, allowing for a more powerful machine [8]. Figure 11 shows the general effect of changing the air gap size on a machine's B-H curve. (B is magnetic field; H is magnetic field strength.)

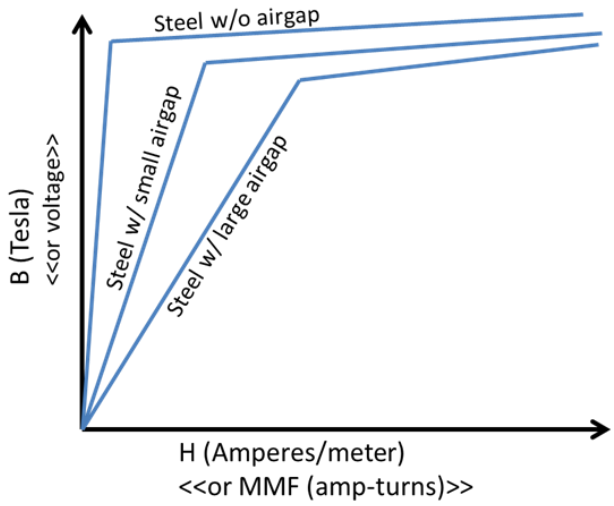

Figure 11: B-H curve with changing air gap

2.2.10: Rotor Pole

The number of magnetic poles (twice the number of pole pairs) in a machine affects various aspects of the machine. The frequency is directly proportional to the number of poles, as described in Equation 5. The magnetic area gap per pole and pole pitch (distance between adjacent poles) are also affected by the number of poles. The parameter of slots per pole per phase is also affected, and the nature of this design consideration is discussed in Section 2.2.12.

Increasing the number of poles reduces required stator and rotor yoke thickness, as described by Equation 9 and shown in Figure 12. [11]

$$t_y = \frac{B}{B_y}\frac{\pi D}{4p} \tag{9}$$

$$B = magnetic\ loading$$
$$B_y = peak\ yoke\ flux\ density$$
$$D = rotor\ outer\ diameter$$
$$p = \#\ poles$$

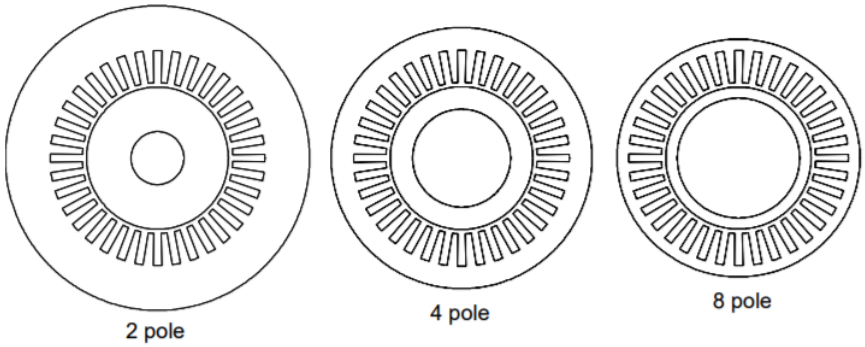

Figure 12: Effect of changing number of poles on stator and rotor yoke thickness [11]

On the other hand, a higher number of poles increases stator iron losses, as iron loss density is roughly proportional to the square of the frequency (which was seen in Equation 5 to be proportional to the number of poles). [11]

A rotor can either be salient pole or cylindrical. In a salient pole rotor, individual rotor poles extend outward from the rotor core. To form an electromagnet, concentrated windings are wrapped around the poles. A salient pole design is characterized by a non-uniform air gap, many poles, and larger rotor diameters. A cylindrical rotor design, on the other hand, consists of distributed windings in slots in the rotor. This allows for the electromagnet to be produced while maintaining the cylindrical shape of the rotor. A cylindrical rotor design is characterized by a near-uniform air gap, fewer poles, smaller rotor diameters, and higher speeds. The salient pole design is very common in aerospace

wound field machines. Figure 13 is a comparison of cylindrical and salient pole rotors. [8]

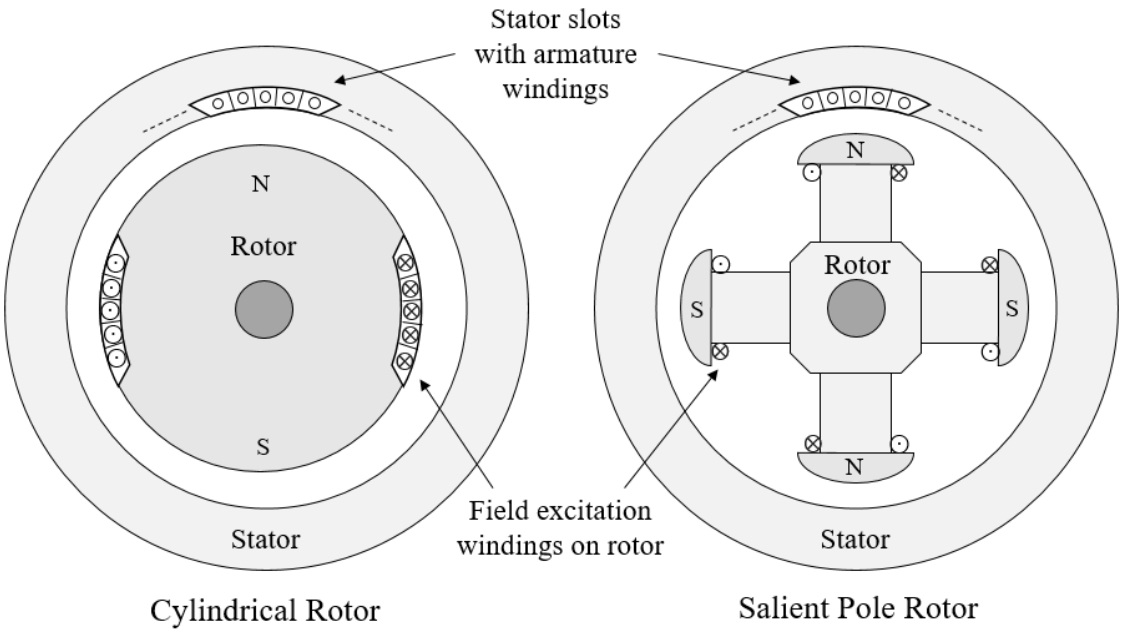

Figure 13: Comparison of cylindrical and salient pole rotors

Another aspect to consider in rotor design is pole embrace. The pole embrace of a machine is the percent of the total rotor diameter that is covered by poles. This value affects the magnetic area gap per pole and pole pitch.

2.2.11: Number of phases

The number of phases in a machine affects various aspects, including the number of stator slots, the slots per pole per phase (see Section 2.2.12), and the per-phase rms current. The number of stator slots can be calculated by:

$$N_S = N_\varphi N_P \tag{10}$$

$$N_s = \#\ stator\ slots$$
$$N_\varphi = \#\ phase\ turns$$
$$N_P = \#\ phases$$

The per-phase rms current is calculated by:

$$I_{\Phi,rms} = \frac{P}{VN_P} \tag{11}$$

$$I_{\Phi,rms} = per-phase\ rms\ current$$
$$P = power$$
$$V = voltage$$
$$N_P = \#\ phases$$

So, according to Equation 10, an increase in the number of phases causes an increase in the number of stator slots. With diameter held constant, an increase in the number of stator slots will decrease the available slot width, causing a decrease the maximum coil width and thus a decrease in the maximum permitted current. At the same time, according to Equation 11, needed current decreases with an increase in the number of phases since the phases are in parallel. This phenomenon has a direct effect on the number of turns needed to sufficiently generate the desired voltage. The number of phases is also used in calculating armature reactions and losses.

2.2.12: Slots per pole per phase

The number of slots per pole per phase (slots/pole/phase) helps govern the association between the poles and the windings. The slots/pole/phase also affects the shape of the back EMF. It is determined by:

$$m = \frac{N_s}{2pq} \tag{12}$$

$$m = slots\ per\ pole\ per\ phase$$
$$N_s = \#\ stator\ slots$$
$$p = \#\ pole\ pairs$$
$$q = \#\ phases$$

The machine is considered an integral slot machine when *m* is an integer, and a fractional slot machine when *m* has a fractional part. For an integral slot machine, the overall back EMF is a summation of the individual winding voltages because the coils that make up a given phase winding are in phase. For a fractional slot machine, the overall back EMF is not a direct summation of the individual winding voltages because the windings are not in phase. Thus the net back EMF's shape is different than those of the individual windings. So adjusting the slots/pole/phase can affect the cleanliness of the sinusoidal voltage output waveform. [8]

The number of slots per pole for assumptions used in this thesis should be a whole number plus 1/2 [6]. This fractional slot winding design allows for the flux under the pole and the total reluctance of the air gap to be about the same, no matter the rotor position. [6]

2.2.13: Winding Configurations

Since voltage is induced on the stator windings, the windings are configured as to help create a sinusoidal back EMF in order to eliminate harmonics beyond the 1st harmonic (the desired fundamental frequency). Harmonics are naturally present within a machine, and can also occur due to loads. Even harmonics can be eliminated by setting the number of stator slots to be a multiple of three (assuming the machine is electrically balanced). But odd harmonics still remain. Elimination techniques help to reduce these harmonics, at the cost of efficiency and increased volume/weight. Winding configurations are typically independent of a machine's physical size. Traditionally, there are three winding configuration factors, simultaneously employed: pitch, distribution, and skew. The total winding factor, k_w, is the net result of the individual derived winding

factors. Ideally, k_w is near 0 for all the odd harmonics beyond the 1st harmonic. Conversely, k_w should be near 1 for the 1st harmonic. From a practical sense, however, k_w is less than 1 for the 1st harmonic due to the nature of the individual winding factors' equations. Equation 13 shows k_w is obtained through a direct multiplication of the individual factors for each harmonic, *n*. [6], [15]

$$k_{w(n)} = k_{p(n)}\, k_{d(n)} k_{sk(n)} \tag{13}$$

$$\begin{aligned} k_w &= winding\ factor \\ k_p &= pitch\ factor \\ k_d &= distribution\ factor \\ k_{sk} &= skew\ factor \end{aligned}$$

- Pitch Factor

  The pitch factor is the ratio of the back EMF of a fractional-pitch winding to that of a full-pitch winding. The pitch factor is dependent on the pitch angle, the angular displacement between two coils. When the pitch angle is 180°, the winding is full-pitched, and thus the resultant phasor sum EMF is a direct arithmetic sum of the induced voltages on both coils. When the pitch angle is less than 180°, the winding is short- or fractional-pitched. The EMF phasor sum is less than a direct sum. So the pitch factor, k_p, can also be defined as the ratio of the coil side EMF phasor sum to the coil side EMF arithmetic sum [5]:

$$k_p = \frac{back\ EMF\ of\ fractional-pitch\ winding}{back\ EMF\ of\ full-pitch\ winding}$$

$$= \frac{coil\ side\ EMF\ phasor\ sum}{coil\ side\ EMF\ arithmetic\ sum} \tag{14}$$

  This ratio can be further defined and put in terms of individual harmonics, n [15]:

$$k_{p(n)} = \sin\left[(n)(\%\, pitch)\left(\frac{\pi}{2}\right)\right] \tag{15}$$

The pitch ratio is the ratio of the pitch angle to a full 180° displacement of two coil sides, which is also the ratio of the pole throw (T_{pole}, the coil span for a given phase in terms of number of slots) to the slots per pole (N_{sp}).

$$pitchRatio = \frac{pitchAngle}{180°} = \frac{T_{pole}}{N_{sp}} \tag{16}$$

Figure 14 shows the pitch factor as a function of pitch ratio for up to the 15th odd harmonic. Since the pitch factor is a ratio, its bounds are [-1, 1], and this factor can be multiplied by a back EMF at a given harmonic to obtain the resultant voltage. At a pitch ratio of 2/3, the pitch factor is 0, and thus odd harmonics that are multiples of 3 (3rd, 9th, 15th, etc.) are eliminated. Thus 2/3 is a good pitch ratio for machine design with three phases. This pitch ratio corresponds to a pitch angle of 2/3×180° = 120°. (Note: a minus sign is placed before $k_{p(n)}$ for certain harmonics in order for all pitch factors to have an end value of 1 with a pitch ratio of 1. Because the power output is AC, the sign of $k_{p(n)}$ does not matter.)

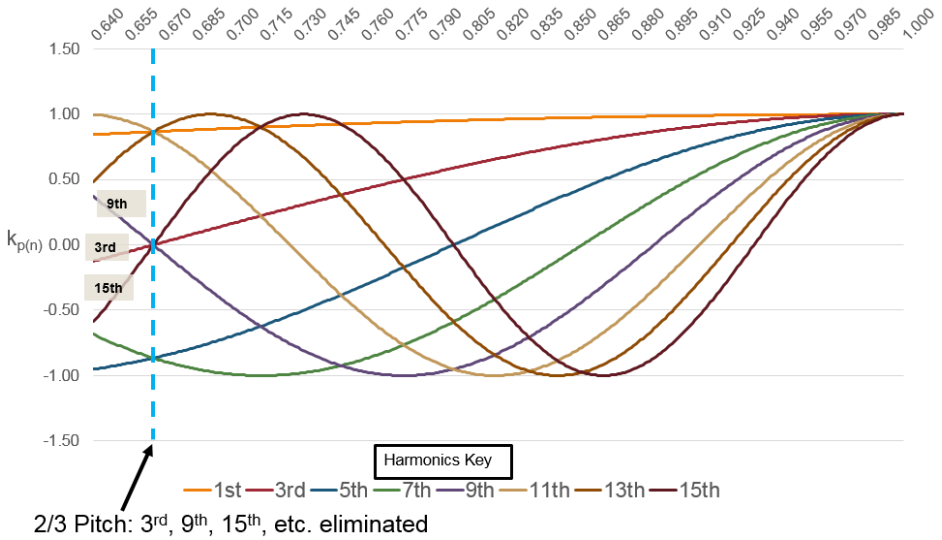

Figure 14: Pitch factor vs. pitch ratio

- Distribution Factor

The distribution factor is the ratio of the induced EMF in a distributed winding to what would be that in a concentrated winding. A concentrated winding consists of all the coil sides placed in one slot, for a given phase and under a given pole. Practically speaking, armature windings are distributed, meaning coil sides for a given phase and under a given pole are placed in different slots. Doing so helps produce a smooth sinusoidal voltage by helping to eliminate harmonics. The distribution factor, k_d, is defined by Equation 17 [5]:

$$k_d = \frac{back\ EMF\ in\ distributed\ winding}{back\ EMF\ in\ concentrated\ winding}$$

$$= \frac{component\ EMF\ phasor\ sum}{component\ EMF\ arithmetic\ sum} \tag{17}$$

This ratio can be further defined and put in terms of individual harmonics, *n* [15]:

$$k_d(n) = \frac{sin(\frac{n\alpha}{2})}{(m)sin(\frac{n\alpha}{2m})} \tag{18}$$

$$m = slots\ per\ pole\ per\ phase$$
$$n = harmonic$$
$$\alpha = phase\ belt\ angle$$

For a phase belt of 120° and 3.5 slots/pole/phase, the odd harmonics that are multiples of 3 (3^{rd}, 9^{th}, 15^{th}, etc.) are eliminated.

- Skew Factor

The skew factor is the derived winding factor that takes into account skewed windings. The hardware design can implement the skew on either the rotor or stator. The skew amount is usually one stator slot pitch. Windings are skewed in order to reduce slot harmonics and reduce cogging (subsynchronous

torques), which occur at high harmonics. Skew does not reduce harmonics as much as distribution and pitch. The skew angle at a given harmonic, *n*, is defined by Equation 19 [15]:

$$k_{sk}(n) = \frac{\sin\left(n\frac{skewAngle}{2}\right)}{n\left(\frac{skewAngle}{2}\right)} \tag{19}$$

Figure 15 is a basic visual of skewed stator slots. The slots are skewed axially along the length of the machine.

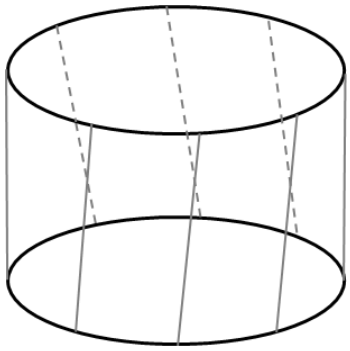

Figure 15: Skewed stator slots

Figure 16 shows the skew factor reducing higher order harmonics as a function of the skew angle, for up to the 21st odd harmonic. With an example of 84 stator slots and 1 slot of skew, the skew angle is 17.1° ^{electrical}. At this angle, for the 19th harmonic (which, due to slot harmonics and cogging, remains after the distribution and pitch factors are taken into account), the skew factor is near 0. Thus, such unwanted harmonic content is nearly eliminated. At the 1st harmonic (the output sinusoidal voltage of interest), the skew factor is near 1, as intended.

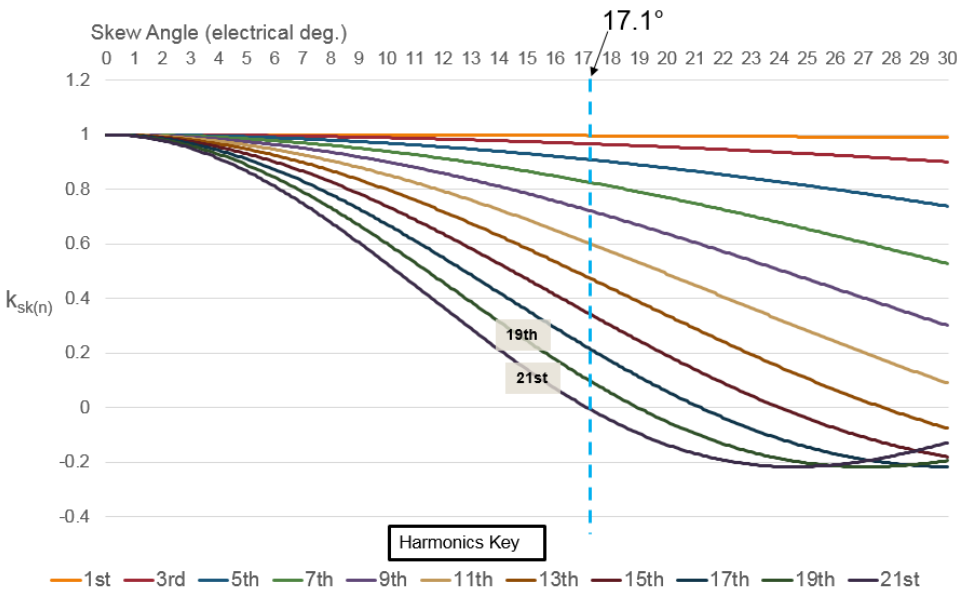

Figure 16: Skew factor vs. skew angle

2.2.14: Open-Circuit Test

To analyze machine performance, a common test performed on generators is an open-circuit (OC) test. For this test, the ampere-turns per pole (or corresponding field current) are swept at no load, and the terminal voltage is measured. Plotting the relation between the no-load terminal voltage and the corresponding amp-turns yields an OC saturation curve. The amplitude of the generated voltage is proportional to frequency and amp-turns (and corresponding field current). [6]

Figure 17 shows a generic OC test plot, which includes the OC curve and the air gap line. The air gap line gives the relationship between the MMF (which is proportional to the field current on the x-axis) and the air gap flux density (which is proportional to the induced OC armature voltage on the y-axis). As the field current increases, the steel begins to saturate. In doing so, it absorbs MMF and causes the percentage of the MMF that reaches the air gap to reduce from nearly 100% (where the air gap line overlays the OC curve) to an increasingly smaller percentage that causes the total induced OC voltage

to drop below the air gap line. The rated voltage is placed in the knee of the curve. Before this point is the linear region, and after this point is the saturation region. Operation in the saturation region is considered inefficient because there are diminishing returns with an increasing field current. [16]

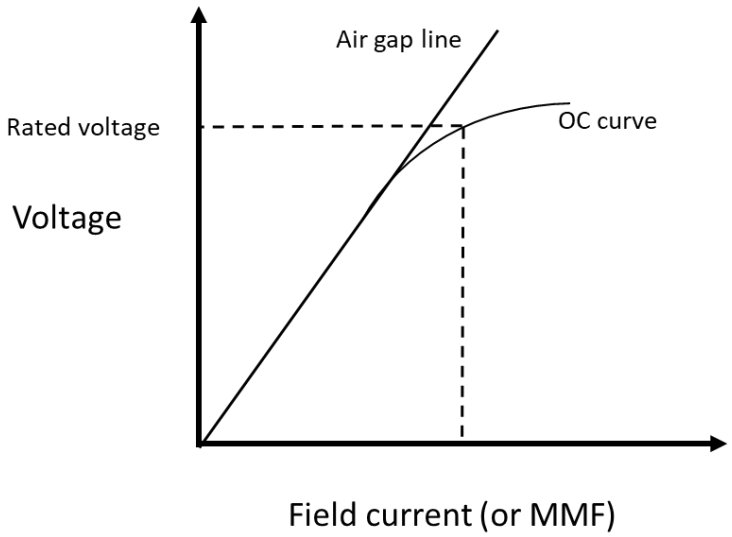

Figure 17: Plot of open-circuit test

2.2.15: Reactances

In an AC circuit, reactance consists of the non-resistive components (inductance and capacitance) of impedance. In an AC circuit arising out of a generator, the reactance will largely be inductance due to the presence of coils. Generator reactances serve two purposes, according to [17]: 1) "calculate the flow of symmetrical short circuit current in coordination studies," and 2) "limit the sub-transient reactance to 12% or less in order to limit the voltage distortion induced by non-linear loads." When a generator's terminals are shorted, the internal voltage and impedance determine the current that flows. Due to the armature reaction on the air gap flux, this current spikes then decays over time to a value dependent upon generator impedances. The generator's resistance is negligible to

its reactance, so only reactance values are considered when dealing with generator impedances. tances.

Table 2 describes the various generator reactances.

Table 2: Generator reactances [17]

Name Importance	Symbol	Range[1]	Effective Time
Sub-transient reactance Determines maximum instantaneous current and current at time molded case circuit breakers usually open.	X''_d	.09 – .17	0 to 6 cycles
Transient reactance Determines current at short time delay of circuit breakers.	X'_d	.13 – .20	6 cycles to 5 sec.
Synchronous reactance Determines steady state current without excitation support (PMG).	X_d	1.7 – 3.3	after 5 sec.
Zero sequence reactance A factor in L-N short circuit current.	X_o	.06 – .09	
Negative sequence reactance A factor in single-phase short circuit current.	X_2	.10 – .22	

[1] Reactances shown are typical per unit values for generators ranging from 40 to 2000 kW.

2.2.16: Losses

Generator losses can be divided into three categories: Copper, Iron (core), and Mechanical [5], [8]:

- Copper losses
  - Armature copper losses (stator)
  - Field copper losses (rotor)
- Iron (core) losses
  - Hysteresis losses (laminations)
  - Eddy current losses (laminations)
- Mechanical losses
  - Friction losses (bearings)
  - Windage losses (rotor pumping)

Chapter 3: Conceptual Sizing Tool

The conceptual sizing tool, written in MATLAB, uses sizing techniques, such as design equations and assumptions from rule-of-thumb metrics, to solve for generator properties and size specifications. Major sources for this program are [6], [13] and [15]. Key inputs are: power, voltage, power factor, overload rating, current density, number of phases, number of poles, speed (continuous and maximum), slot to tooth ratio, and steel type. Key outputs for the model are: physical dimensions, harmonics, losses, generated voltage, volume/weight estimates, and armature reactions. The L/D ratio can either be an input or output.

The model allows the user to ignore design points inputted by the user that have unreasonable calculations. Any or all of the violation checks can be enabled by the user, which are performed immediately after the sizing code is run. There are three such violation checks:

- Insufficient slot width: The stator slot must be of sufficient width for the conductor to fit. The width of the conductor is determined by the machine's rated current and the permitted current density of the wire, which is an input and can change based off whether the machine is air cooled (lower current density) or oil cooled (higher current density).
- Tip speed over limit: the tip speed of the machine should not go beyond a set limit, which was stated in Section 2.2.6 to be 650 fps.
- Unreasonable length to diameter ratio: if the L/D ratio is calculated, it should be within a given window, stated in Section 2.2.6 to be 0.3 – 2.0.

3.1: Algorithm

Figure 19 is a flow chart that summarizes the model's algorithm.

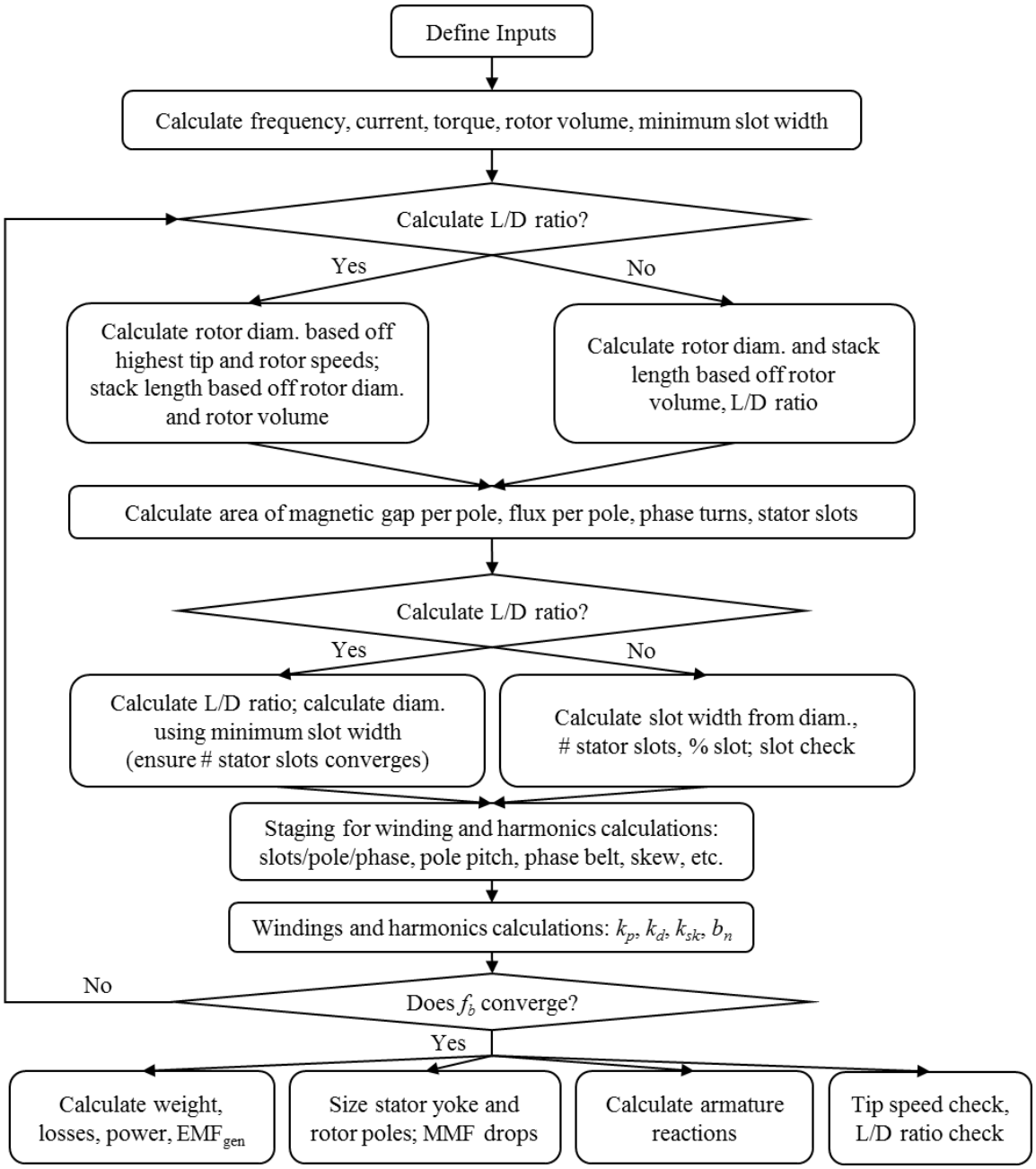

Figure 18: Generator sizing tool flowchart

This algorithm is now described in detail. First, input parameters are defined. Next, important parameters in sizing the machine are calculated: frequency, current, torque, and rotor volume. The minimum wire width (obtained from highest envisioned current and current density) and corresponding slot width is also calculated. If copper is selected as the wire type, the user has the option of using wire tables to round the minimum necessary copper width up to the available gauge width. The minimum slot width is subsequently determined by adding insulation width to the minimum copper width.

Next, the program enters a loop that will attempt to converge f_b, the form factor. The form factor is the penalty paid for good sinusoidal power quality, in the form of effective turn reduction on the armature winding. It is the ratio of the effective (or rms) value to the average value of the flux wave [6]. The starting assumption for f_b is 0.7, which is likely near its output value for a given set of inputs. As stated earlier, the program gives the user the option to either input or calculate the L/D ratio. Within the loop, if the L/D ratio is an input, the rotor diameter is calculated as a function of the rotor volume and L/D ratio (*ldr*):

$$d_{rotor} = \left(\frac{4V_{rotor}}{\pi \times ldr}\right)^{\frac{1}{3}} \tag{20}$$

If the L/D ratio is chosen to be calculated, then rotor diameter is calculated based off the envisioned highest rotational speed (ω_{high}) and the maximum allowable tip speed of the machine (v_{max}):

$$d_{rotor} = 2\frac{v_{max}}{\omega_{high}} \tag{21}$$

The rotor diameter, stator inner diameter, and corresponding circumference are subsequently calculated. If the L/D ratio is an input, the rotor stack length is calculated by:

$$l_{stack} = ldr \times d_{rotor} \tag{22}$$

If the L/D ratio is an output, the stack length is calculated by:

$$l_{stack} = \frac{V_{rotor}}{\pi \left(\frac{d_{rotor}}{2}\right)^2} \tag{23}$$

Next, the magnetic effective stack length (based on the fact that the steel is made of lamination stacks with thin insulation) is calculated, and from that, the magnetic area gap per pole (A_{mp}) is determined based off the rotor circumference (C_{rotor}), effective stack length (l_{eff}), pole embrace (λ), and number of poles (p).

$$A_{mp} = C_{rotor} \frac{l_{eff}\lambda}{p} \tag{24}$$

The air gap flux density, B_{gap}, is determined by the product of the maximum teeth flux density ($B_{teeth,\ max}$) and the percent of the tooth width ($\%_{\ tooth}$) of the summed slot and tooth width:

$$B_{gap} = B_{teeth\ max} \times \%_{tooth} \tag{25}$$

The flux per pole, Φ_{pole}, is then calculated as the product of A_{mp} and B_{gap}:

$$\Phi_{pole} = A_{mp} \times B_{gap} \tag{26}$$

The number of phase turns per pole pair ($N_{\varphi,\ pair}$) is now calculated as a function of various parameters: operation voltage (V), f_b, frequency (f), Φ_{pole}, and p. The ⌈ ⌉ bracket entails a ceiling operator that rounds up the calculation to the nearest whole number.

$$N_{\varphi,pair} = \left\lceil \frac{V}{4 f_b f(\Phi_{pole})(10^{-5})\left(\frac{p}{2}\right)} \right\rceil \quad (27)$$

$N_{\varphi,\,pair}$ gives way to the total number of phase turns, N_φ:

$$N_\varphi = N_{\varphi,pair} \times \frac{p}{2} \quad (28)$$

The number of stator slots (N_s) is the product of the number of phases (φ) and N_φ. Although the slot width to tooth width ratio can be adjusted, the number of stator teeth (N_t) is always equal to N_s.

$$N_s = N_t = \varphi \times N_\varphi \quad (29)$$

If the L/D ratio is an input, the slot width (w_{slot}) is calculated by:

$$w_{slot} = \frac{C_{inner\ stator}}{N_s}(\%_{tooth}) \quad (30)$$

$$C_{inner\ stator} = inner\ circumference\ of\ stator$$

The slot width violation check is now performed to determine if the stator slot is of sufficient width.

If the L/D ratio is an output, the user has the option of calculating for the minimum rotor diameter (and corresponding L/D ratio), as opposed to using the diameter that would produce the maximum possible tip speed at the given highest envisioned rotor speed. This is done by setting the slot width equal to the minimum slot width, and subsequently using this width and the given stator slots to back out $C_{inner\ stator}$. In doing so, the stack length changes, causing a cascade of recalculations (see Equations 24 – 29). The number of stator slots (N_s) can thus potentially change. So these recalculations are done in a loop to provide a feedback for N_s; the loop breaks when N_s converges.

The slot depth is calculated based off the minimum wire width and the assumption of two conductors per slot.

Staging is now done for the windings and harmonics calculations. The slots per pole and slots/pole/phase are determined by dividing out the number of slots with the number of poles and then with the number of phases, respectively. The pole throw (T_{pole}) is equal to the number of whole teeth per pole (N_{tp}). Equation 31 shows how these values are determined. The ⌊ ⌋ bracket entails a floor operator that rounds down the calculation to the nearest whole number.

$$T_{pole} = N_{tp} = \left\lfloor \frac{C_{rotor}\lambda}{p \times 2w_{slot}} \right\rfloor \tag{31}$$

The pitch ratio was found in Equation 16 to be the ratio of the pole throw to the number of slots per pole (N_{sp}).

$$pitchRatio = \frac{pitchAngle}{180°} = \frac{T_{pole}}{N_{sp}} \tag{16}$$

The phase belt angle (in degrees) is calculated by:

$$phaseBeltAngle = \frac{180}{N_{sp}}\lambda \tag{32}$$

The skew angle (in degrees) is calculated by:

$$skewAngle = slotsSkew \times \frac{180}{N_{sp}} \tag{33}$$

Harmonics calculations are then performed, as was described in Section 2.2.13. f_b is calculated, and compared to the original f_b. Once f_b converges, the loop terminates and the highest envisioned tip speed (v_{high}) is calculated based off the highest envisioned rotational speed (ω_{high}) and d_{rotor}:

$$v_{high} = \omega_{high} \times \frac{d_{rotor}}{2} \tag{34}$$

v_{high} is then compared to the maximum allowable tip speed (v_{max}) to check if there is a tip speed violation. The L/D ratio violation check is also performed for the given window.

Next, MMF drops are calculated. Figure 19 shows a simplified magnetic circuit of the generator, and approximately where the reluctances labeled in the circuit are on the machine. $R_{r\text{-}yoke}$ stands for reluctance of rotor yoke, $R_{r\text{-}pole}$ stands for reluctance of rotor pole, $R_{s\text{-}core/yoke}$ stands for reluctance of stator core (also known as the yoke), $R_{s\text{-}teeth}$ stands for reluctance of stator core teeth, and R_{gap} stands for reluctance of air gap.

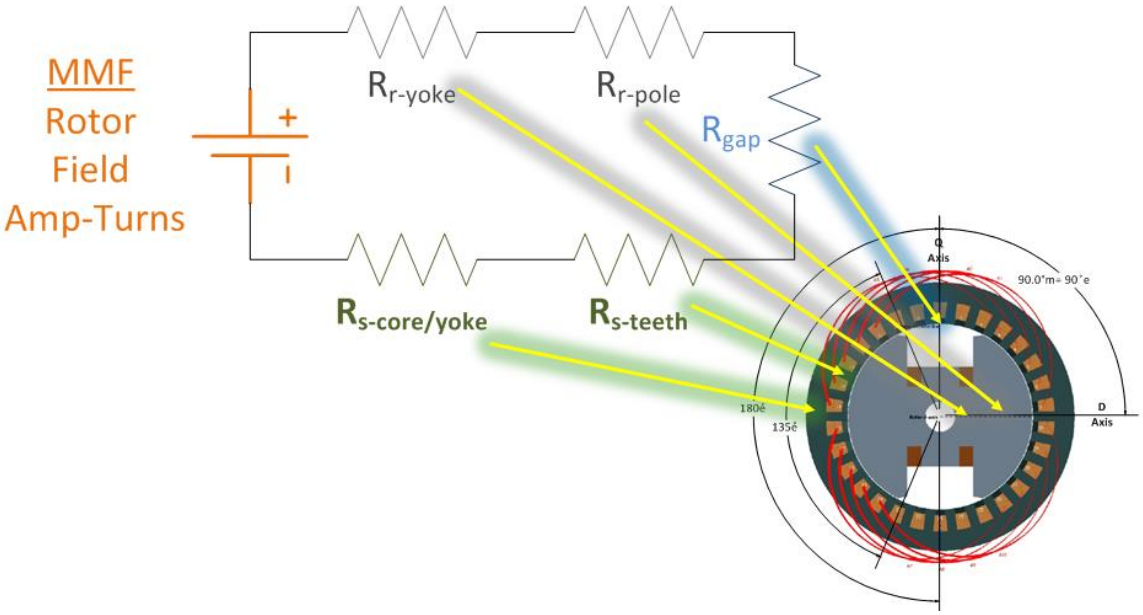

Figure 19: Magnetic circuit of generator

The flux through the magnetic circuit is limited by the stator teeth. The various magnetic flux path lengths for each reluctance type are determined by the geometries associated with the given reluctance type. The air gap is unique among these magnetic circuit components in that its B-H (magnetic flux density to magnetic field strength) relationship is a straight line, rather than a curve associated with that of steel's B-H

relationship. The total MMF drop is the sum of the MMF drops throughout the circuit, including the air gap. Similarly, the total reluctance is the sum of the reluctances throughout the circuit, including the air gap.

The output voltage can now be calculated. It was given in Equation 4 as:

$$E = \sqrt{2}\pi f_b N_\varphi f \Phi \tag{4}$$

Next, the armature reactions are determined: direct axis armature reactance and quadrature axis armature reactance. The armature leakage reactances are then calculated: slot reactance, zig-zag leakage reactance, end-connection leakage reactance, and belt leakage reactance. These reactances are summed to obtain the total leakage reactance. The unsaturated synchronous reactances are then determined: the direct axis unsaturated synchronous reactance is the sum of the total leakage reactance and the direct axis armature reactance; the quadrature axis unsaturated synchronous reactance is the sum of the total leakage reactance and the quadrature axis armature reactance.

Weight is determined by estimating the total stator and rotor volume, and using "fudge factors" to obtain a weight, given that of a known 40 kVA generator available for laboratory testing. Finally, power losses and power densities are determined. Stator I^2R, eddy, pole face, and friction/windage losses are estimated. (These loss estimates are to be improved upon, and the other power losses have not yet been determined in this sizing tool.) Power densities give the user the following ratios: lb/kW, kW/lb, kg/kW, kW/kg, N-m/kW, and kW/N-m.

3.2: 40 kVA Example

To determine if the generator sizing code can be used for preliminary machine design optimization and analysis, a known generator design should be run in the model. The model outputs can be compared to the actual generator properties, and doing so allows one to baseline the sizing code. Thus a single-speed 40 kVA aircraft generator, like that described in [18], is chosen as an example for the model. Many aspects and dimensions (and all model input parameters) of this example are known. To analyze for an optimal generator design, all input parameters are constant except for the air gap shear stress and the L/D ratio of the generator. Even though both these parameters are known, they are swept to test the program by determining if it can produce a design near the actual hardware design. Table 3 lists key input properties for this generator, including the swept and actual values of the shear stress and the L/D ratio:

Table 3: 40 kVA design inputs

Parameter	Value	Units
Continuous Power Rating	40	kVA
Voltage	120	$V_{ph\ rms}$
Power Factor	0.75	
Overload	1.25	
Current Density	20	kA/in^2
Phases	3	
Wire type	copper	
Air Gap Size	20	mils ($1/1000^{th}$ in)
Air Gap Shear Stress	1 – 5 (sweep; actual: 2.88)	lbf/in^2 (psi)
Rotor Speed	6000	rpm
Max Rotor Speed	6000	rpm
Length to Diameter Ratio	0.3 – 2.0 (sweep; actual: 0.579)	
Slot to Tooth Ratio	1	
Stack Factor	0.93	
Slots Skew	1	
Pole Embrace	0.75	
# Poles	8	
Maximum Tip Speed	650	fps
Rotor Steel Type	M-36	
Stator Steel Type	M-36	

The resultant data set for this example has design points at the increments for the swept variables of shear stress and L/D ratio. Figure 20 shows the weight as a function of shear stress and L/D ratio. As the shear stress decreases, the generator is able to handle less TRV, so the volume and thus the weight increases. The L/D ratio does not affect the total weight.

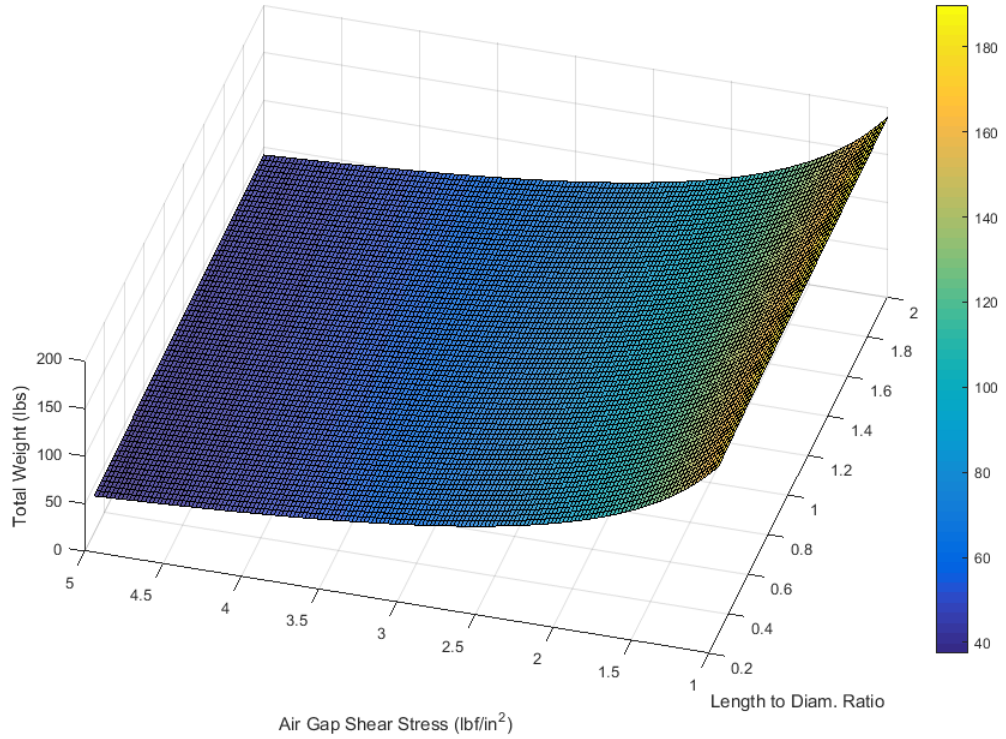

Figure 20: Weight plot for 40 kVA design

Figure 21 shows the number of stator slots as a function of shear stress and L/D ratio. The number of stator slots is a product of the number of phases and number of phase turns, which is inversely proportional to the flux per pole. The flux per pole is proportional to the magnetic area gap per pole, which increases with an increase in L/D ratio. So a decreasing L/D ratio will cause the number of stator slots to increase. The stator slots also increase with shear stress. Increasing shear stress (and corresponding TRV) yields higher torque density and lower volume, according to Equations 35 and 36.

$$V_{rotor} = \frac{\tau_{max}}{\tau_{per\ rotor\ volume}} \tag{35}$$

$$\tau_{max} = \frac{P}{N_{rpm}} \tag{36}$$

A lower volume yields a smaller magnetic area gap per pole, causing the number of phase turns per pole pair to increase. So, with an increase in shear stress, the total number of phase turns increases, causing the number of stator slots to increase.

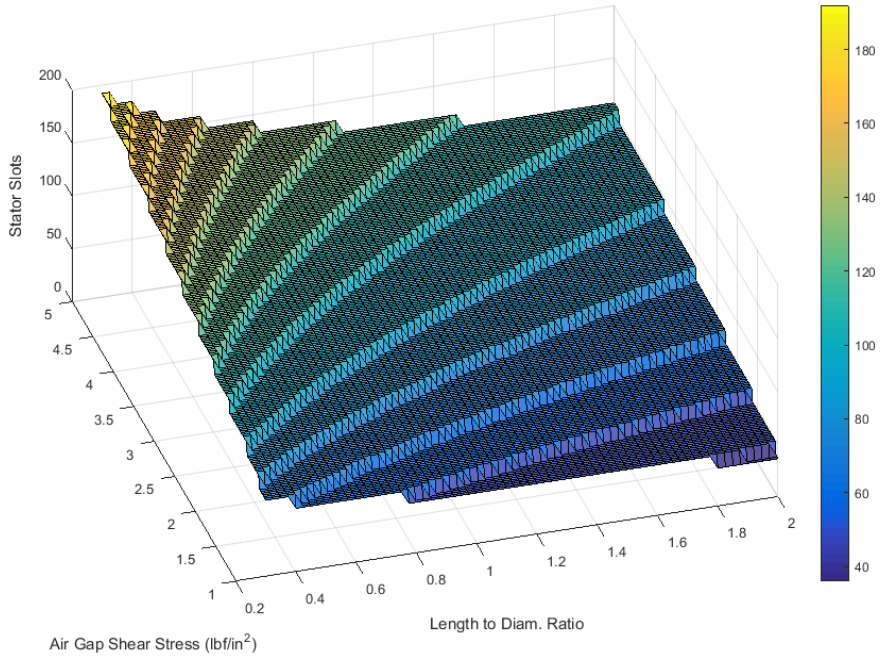

Figure 21: Stator slots plot for 40 kVA design

As explained in Section 2.2.13, the pitch ratio is ideally 2/3. Since this value is ideal but not necessary, the pitch ratio is not part of the violation checks. Figure 22 shows this pitch ratio as a function of shear stress and L/D ratio. A design should be chosen in the dark purple area, where the pitch ratio is 2/3. A point (which is the eventual design point chosen) is labeled in this area.

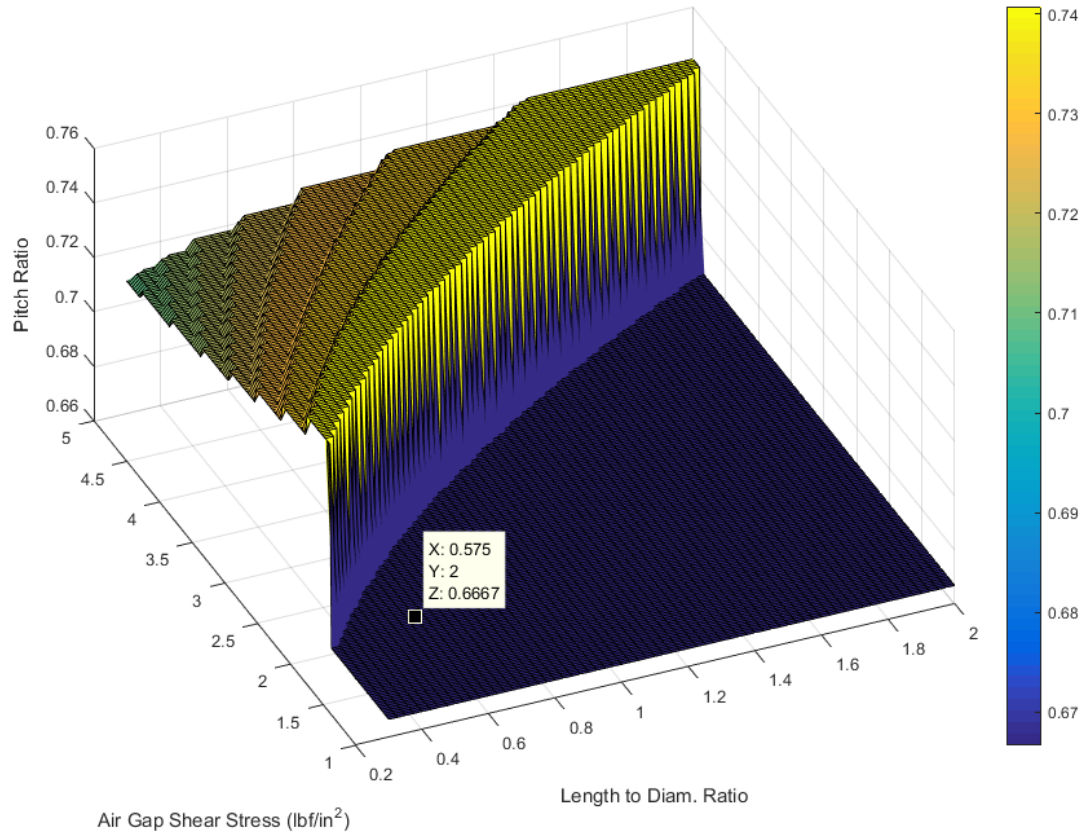

Figure 22: Pitch ratio plot for 40 kVA design

For this example, violation checks for slot width, tip speed, and L/D ratio are now performed. The tip speed does not exceed 650 fps, and there are no unreasonable L/D ratios because the L/D ratio parameter is an input that sweeps 0.3 – 2.0. There are, however, slot width violations. Figure 23 shows (at two different angles) the calculated and minimum slot widths for the design points. For all of them, the minimum slot width is a constant, as this value is not determined by air gap shear stress or L/D ratio. But the calculated slot width does change in sweeping such parameters. So any point at or above the blue plane (the minimum slot width) corresponds to a slot width at or above the minimum slot width, and therefore a reasonable design point. Any point below the blue

plane, however, corresponds to an insufficient slot width and therefore an unreasonable design point.

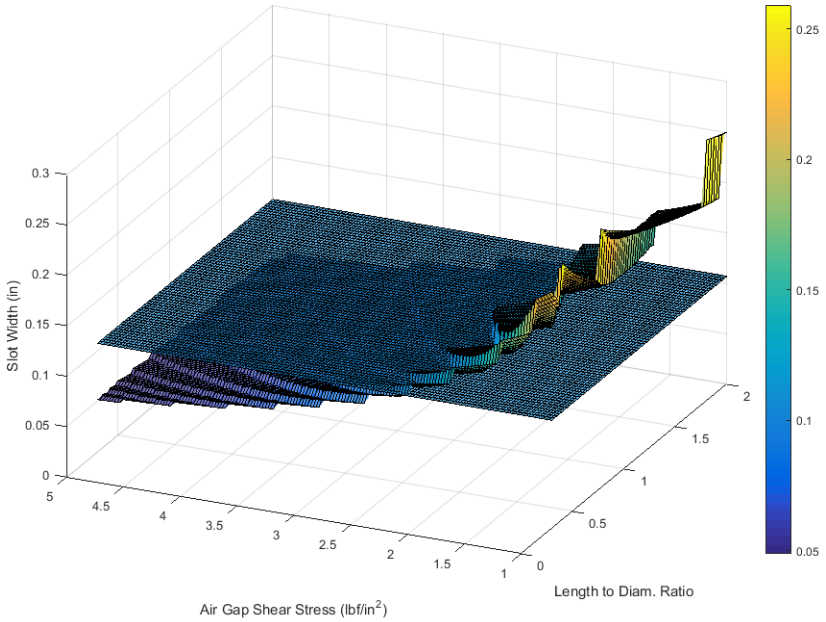

(a)

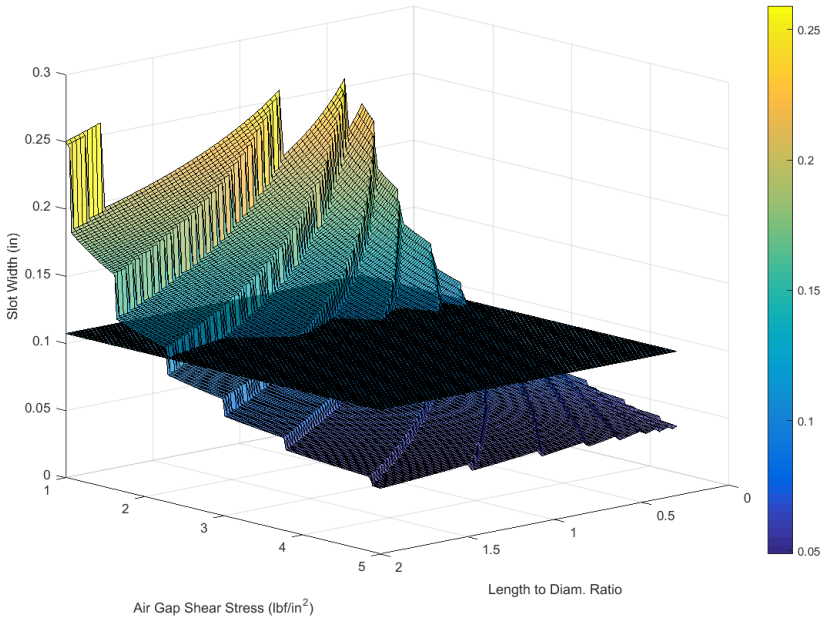

(b)

Figure 23: Calculated slot width overlaid with minimum slot width, shown at two angles (a, b)

Unreasonable calculations are now removed. Figure 24 shows the reasonable design points after the violation check. The checkered white area corresponds to design points without violations, while the black area corresponds to design points with violations (insufficient slot widths, in this example).

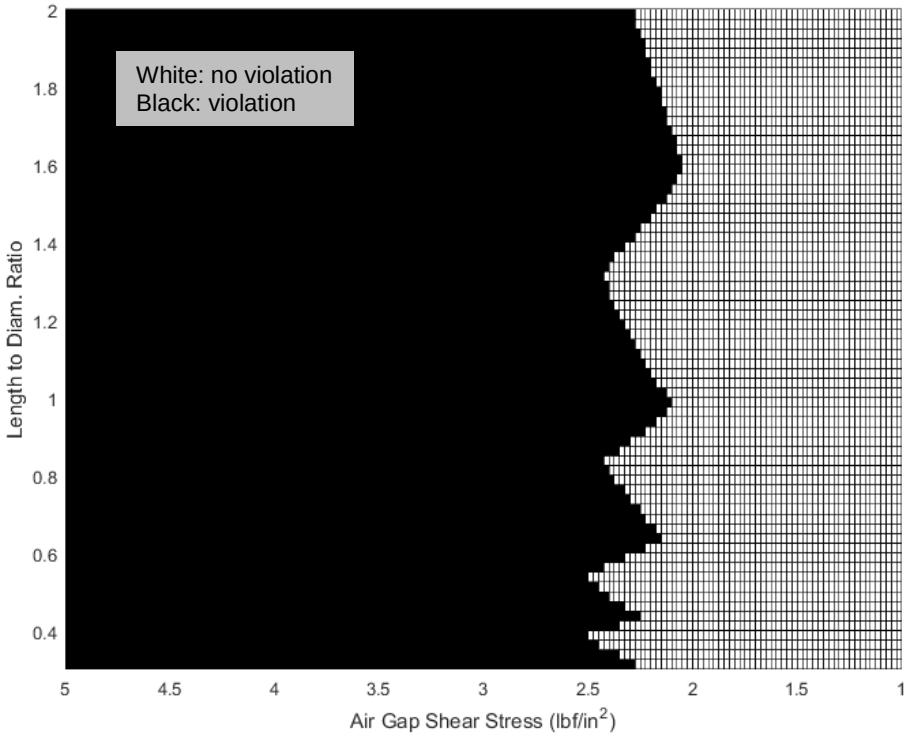

Figure 24: Violation check plot for 40 kVA design (points within black area removed)

Now that the violations have been removed, one can examine more closely the optimal design point for this example. As stated in Section 2.2.12, the number of slots per pole should be a whole number plus 1/2, if possible. The air gap shear stress picked should be a reasonable estimate that errs on the lower end to allow for a more robust air-cooled machine, so a value of 2 psi is chosen. An L/D ratio of 0.575 is then chosen, as this ratio is near the physical hardware's actual ratio of 0.579. This design point yields 3.5 slots/pole/phase (Figure 25), 10.5 slots per pole (Figure 26), and 84 stator slots

(Figure 27). This design point remains after violation checks, so it is a reasonable calculation. Even though the machine's actual air gap shear stress value (emblematic of the cooling capabilities of the machine) is 2.88 psi, 2 psi was chosen to keep the number of stator slots at 84, which is that of the actual machine (2.88 psi would have caused the number of stator slots to jump to 96).

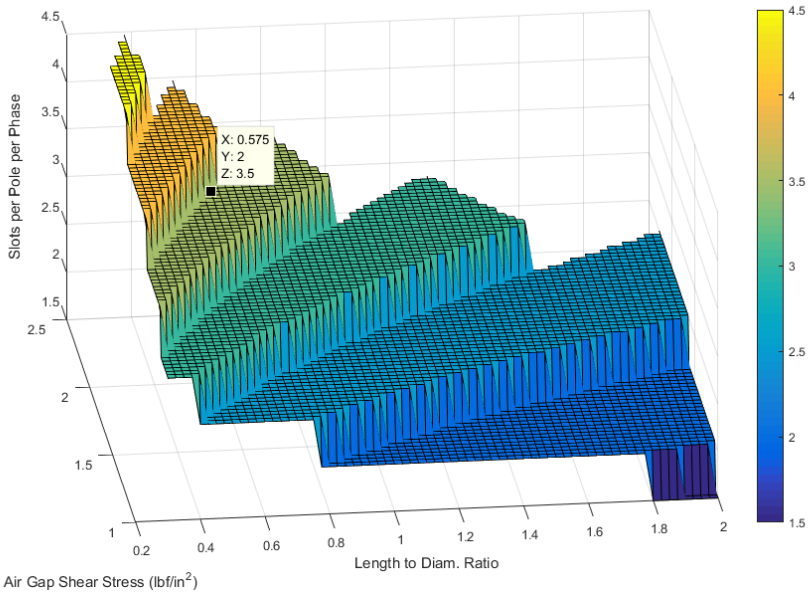

Figure 25: Slots per pole per phase plot for 40 kVA design

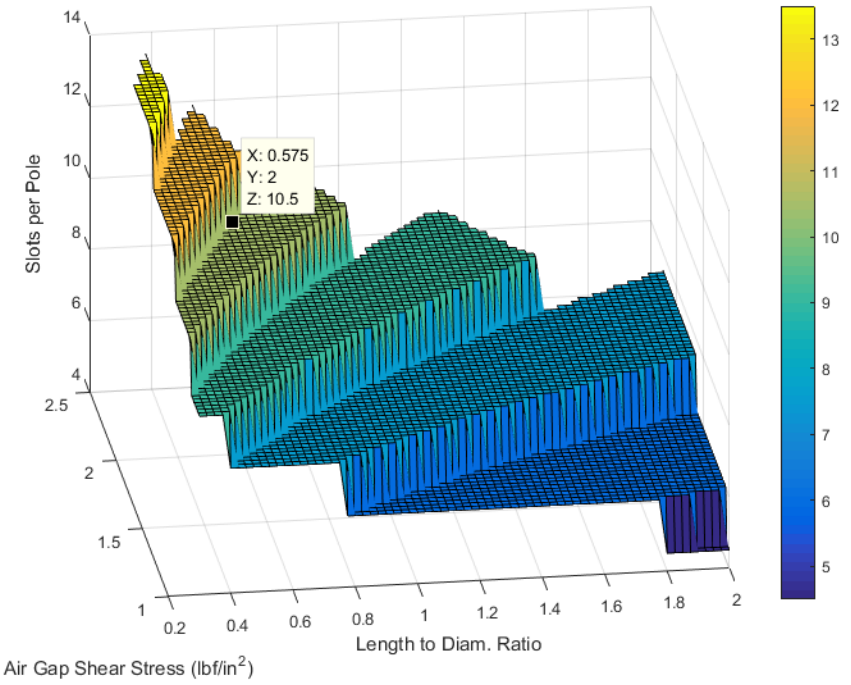

Figure 26: Slots per pole plot for 40 kVA design

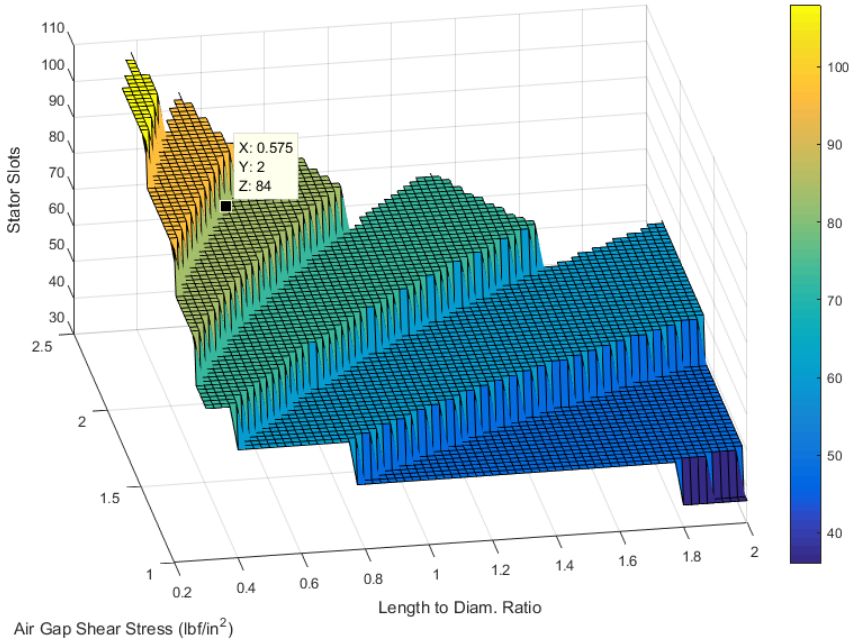

Figure 27: Stator slots plot for 40 kVA design

For this design point, the rotor diameter is 6.8 in. Figure 28 shows that it decreases with an increase in L/D ratio (as the stack length compared to the diameter increases). The diameter also decreases as the air gap shear stress increases because less volume is needed with increased shear stress.

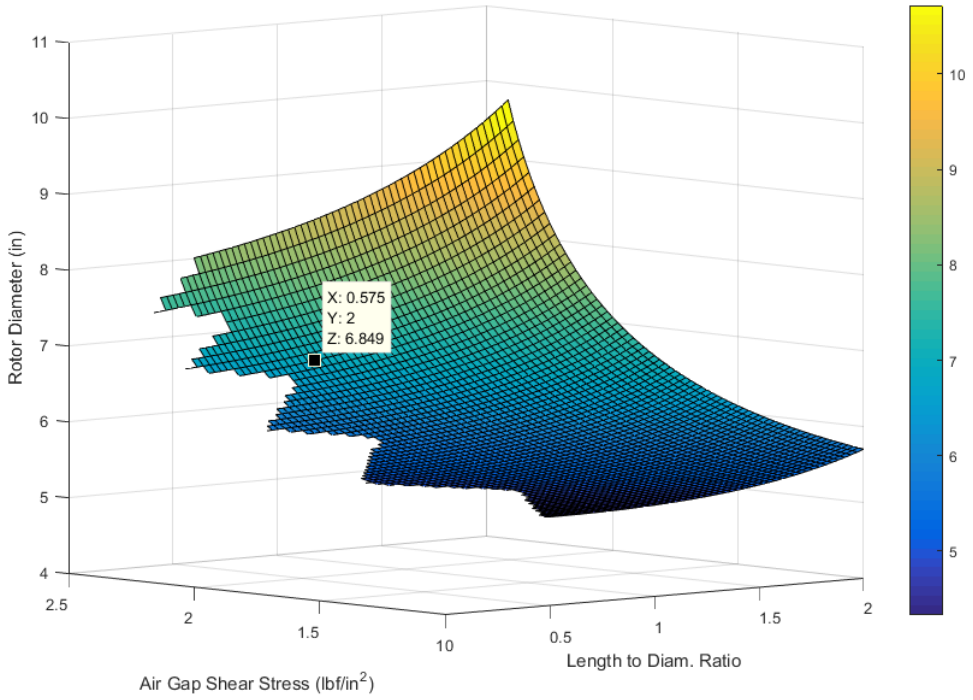

Figure 28: Rotor diameter plot for 40 kVA design

The highest tip speed of the machine is the maximum envisioned tip speed, which is based off the rotor diameter and rotational speed. As stated earlier, it should not exceed 650 fps. As stated earlier, this example is a single-speed machine, so the rotational speed for which it is designed (6000 rpm) is the same as the maximum envisioned rotational speed (6000 rpm). Figure 29 shows that the highest tip speed plot has the same shape as that of the rotor diameter plot because tip speed is directly proportional to rotor diameter. The machine's highest tip speed is about 179 fps, well below the 650 fps limit. The highest tip speed of the swept variable space is 280.6 fps, still well below the 650 fps

limit. Because of this disparity, one might consider setting the maximum tip speed to be closer to the highest tip speed result. Doing so would help emulate any requirements of the generator that are not considered in the 650 fps limit, such as rotating diode limitations and a desire for a more robust machine. Such may have been the case for the generator being modeled in this example: its actual tip speed is 177 fps at its operating speed of 6000 rpm.

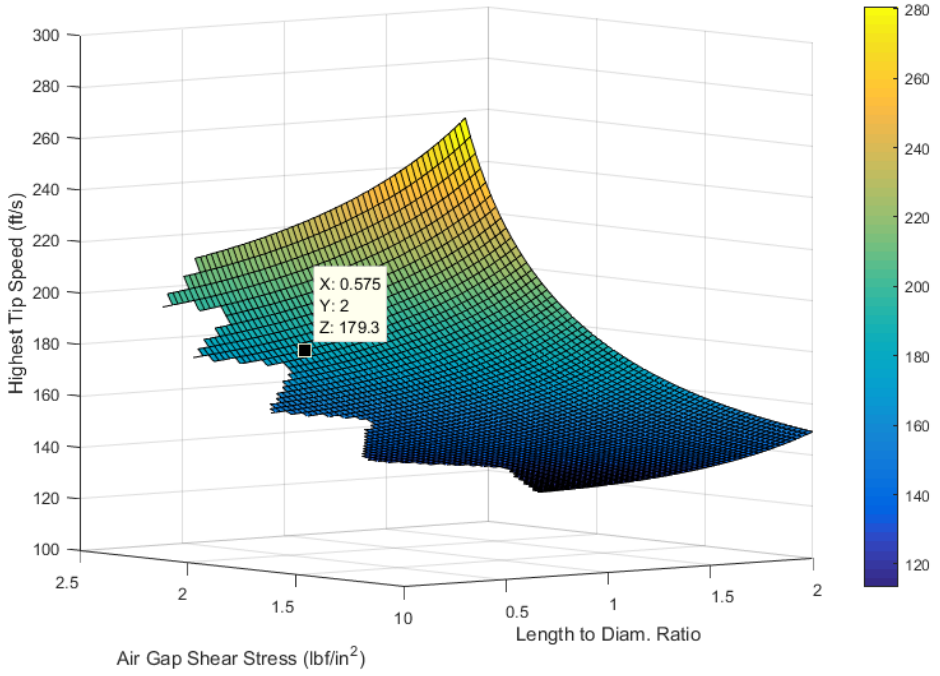

Figure 29: Tip speed plot for 40 kVA design

Figure 30 shows that the stack length increases with L/D ratio (as the stack length compared to the diameter increases). Stack length decreases, however, with shear stress since less volume is needed with more shear stress (and corresponding TRV).

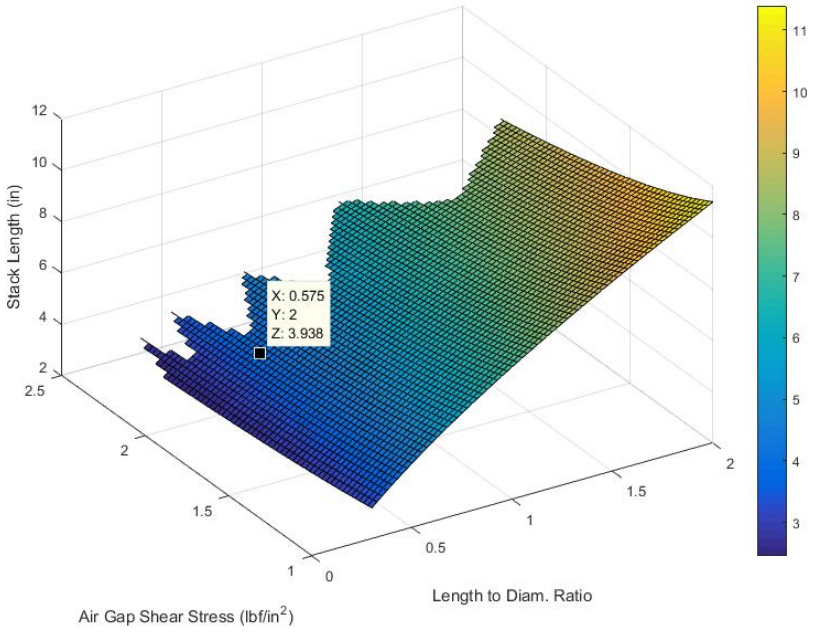

Figure 30: Stack length plot for 40 kVA design

The total weight of the generator is estimated to be 92 lbs. In comparison, the weight of the 40 kVA machine from [18] is 86 lbs.

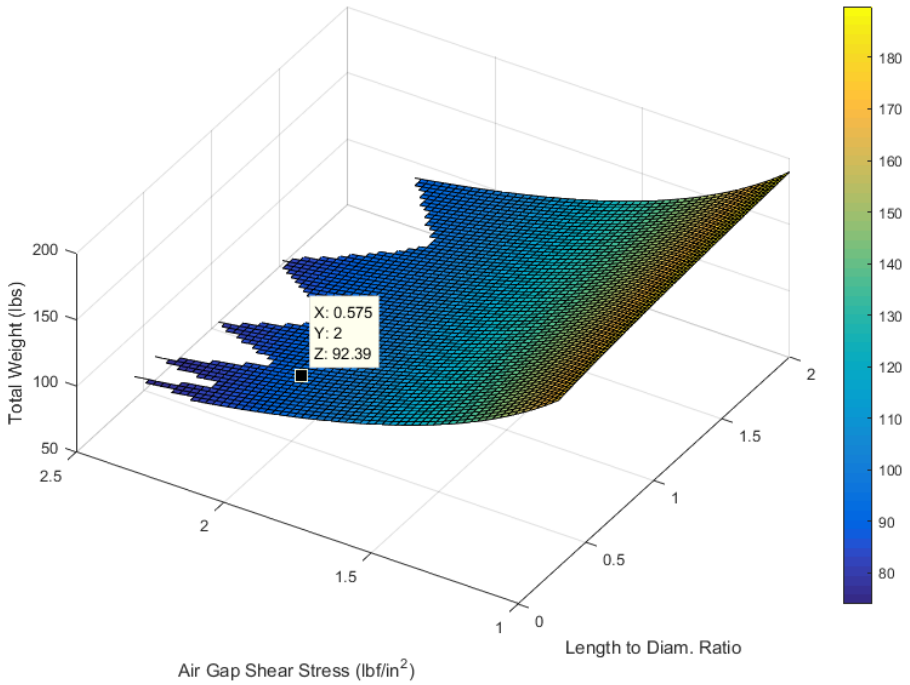

Figure 31: Weight plot for 40 kVA design

For the chosen design point of 2 psi and L/D ratio of 0.575, the machine's OC voltage characteristics are now simulated. On the x-axis the MMF is swept from 0 – 1000 amp-turns (appropriate window for showing the amp-turns necessary on the rotor field to generate the intended OC voltage). In practice, this characterization test for a two-stage machine would have the input DC excitation current for the exciter generator on the x-axis, since the magnetic field strength cannot be measured while the machine is spinning. Although this machine is a single-speed machine, for characterization purposes it is good to simulate the machine operating at speeds lower than 6000 rpm. One reason for this is when starting, the machine has to ramp up to 6000 rpm. Shown in Figure 32 are the OC voltage curves for the machine at five speeds and corresponding frequencies, ranging from 3000 – 6000 rpm (200 – 400 Hz). The output voltage curves rise with speed/frequency and magnetic flux, which increases with magnetic field strength. These two phenomena can be confirmed by Equation 4:

$$E = \sqrt{2}\pi f_b N_\varphi f \Phi \tag{4}$$

The steel in the machine starts to saturate at an input magnetic field strength of about 350 amp-turns, which can be seen by a bend in the output voltage. As explained in Section 2.2.14, any machine operation past this point is inefficient because there are diminishing returns: the back EMF increases by less than before as the input MMF increase beyond about 350 amp-turns. These diminishing returns are due to core losses within the steel. For the 6000 rpm operating point plot, the saturation voltage should be at 120 V since 120 V is the input design parameter of this example. This simulation, however, only shows the voltage reaching about 110 V before saturation.

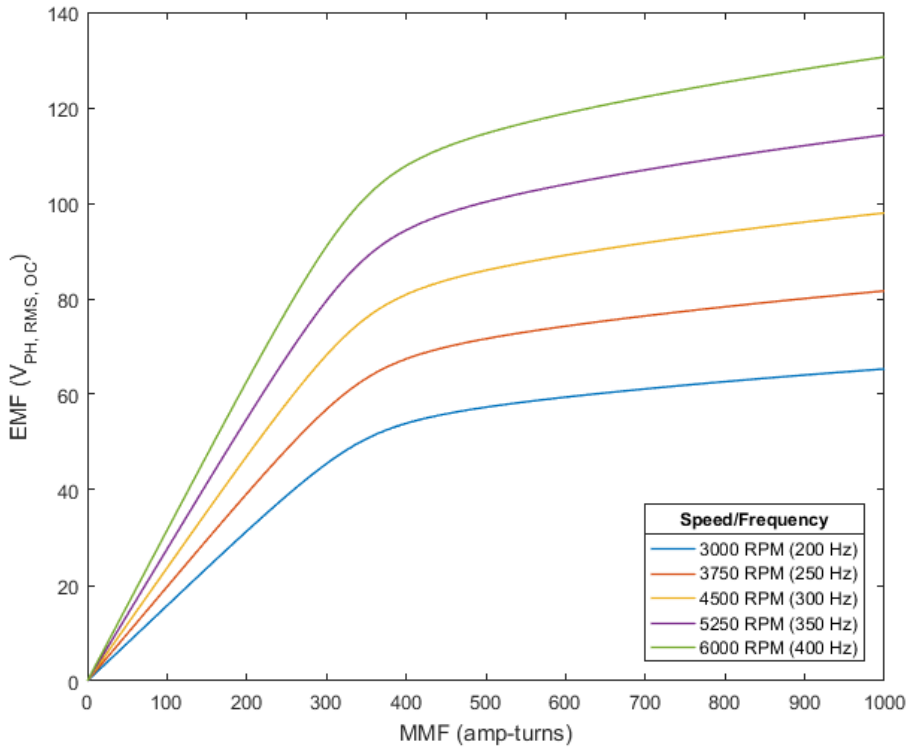

Figure 32: OC saturation plot for 40 kVA design (L/D ratio = 0.575, shear stress = 2 psi)

As was seen in Figure 27, the design point chosen (x: L/D ratio = 0.575, y: shear stress = 2 psi) is near the point where the number of stator slots jumps from 84 to 96. This jump can occur at (x: L/D ratio = 0.575, y: shear stress = 2.05 psi). The jump is emblematic of the number of phase turns per pole pair jumping from 7 to 8, which means the number of phase turns, N_φ, jumps from 28 to 32. According to Equation 4, the output voltage is proportional to N_φ. So once this jump occurs, the machine does not saturate until about 120 V. But after jumping down from 32 to 28 phase turns, f_b remains essentially the same at 0.814, and the magnetic flux, the only other aspect of Equation 4 that can change in adjusting shear stress or L/D ratio, does not yet have a chance to make up for the lost phase turns. A design point of (x: L/D ratio = 0.575, y: shear stress = 1.7 psi) was chosen, which is further from the jump up in stator slots. The OC voltage plot of

this design point saturates at about the desired 120 V instead of 110 V. So if the expected saturation voltage is not obtained for a given design point, one should move the selection further from where the number of stator slots would jump.

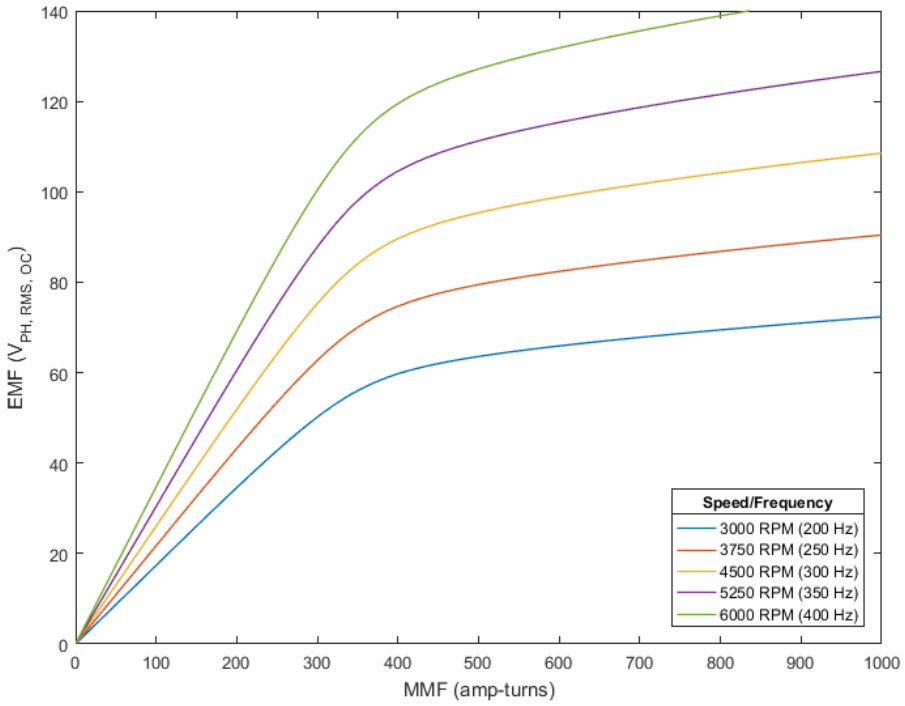

Figure 33: OC saturation plot for 40 kVA design (L/D ratio = 0.575, shear stress = 1.7 psi)

For M-36 steel, this program by default assumes the maximum teeth flux density to be 90 klines/in^2 and the maximum stator flux density to be 95 klines/in^2. These values, however, are rules of thumb, and are thus adjusted to determine if changing them will affect the OC voltage curve. For the 40 kVA design points of (x: L/D ratio = 0.575, y: shear stress = 2 psi), the maximum teeth and stator flux densities are changed to 80 and 85 klines/in^2, respectively. Doing so changes the number of stator slots to jump from 84 to 96, which means N_φ jumps from 28 to 32. The OC voltage plot in Figure 34 shows the saturation occurring near 120 V, similar to how the saturation is at 120 V due to increasing the shear stress to above 2.05 psi, as explained in the previous paragraph. The

maximum teeth and stator flux densities are then changed to 100 and 105 klines/in^2, respectively. Figure 34 shows that the OC saturation curve of these flux densities is very close to that of the original maximum teeth and stator flux densities of 90 and 95 klines/in^2, respectively. In such a plot, increasing from 90 and 95 klines/in^2 to 100 and 105 klines/in^2 does not cause N_φ to jump, unlike decreasing from 90 and 95 klines/in^2 to 80 and 85 klines/in^2. This plot shows that changing the maximum teeth and stator flux densities does not cause a significant change in the OC voltage saturation curve, unless such a change yields a jump in N_φ (which, as explained earlier, is caused by a jump in the number of phase turns per pole pair).

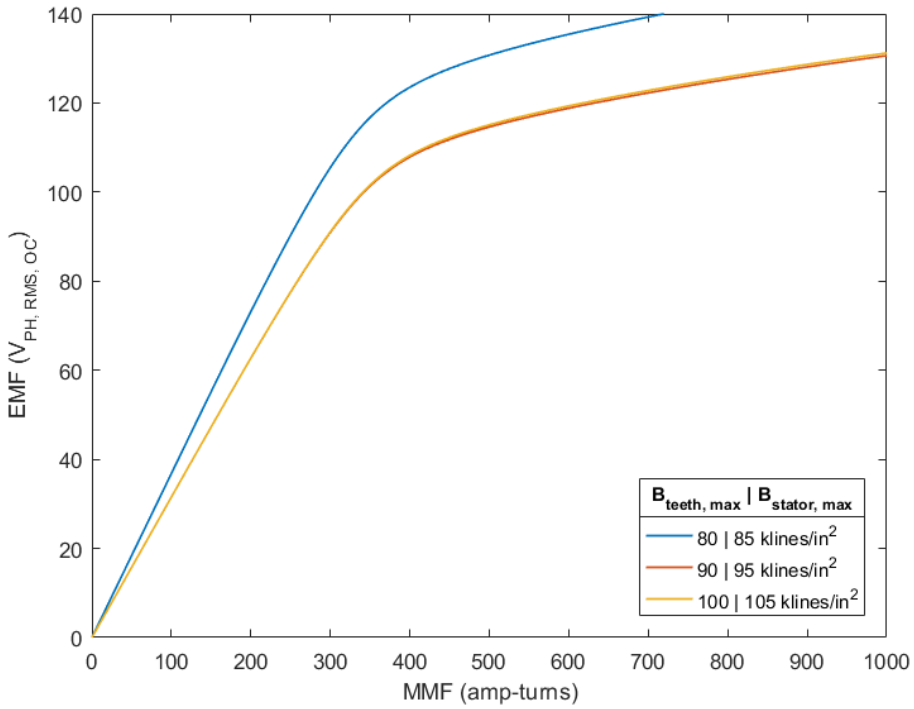

Figure 34: OC saturation plot for 40 kVA design with selected flux densities

As explained in Section 2.2.9, an increase in air gap size allows for better output voltage regulation. This phenomenon can be seen in Figure 35: as the air gap size is swept from 20 – 50 mils (in increments of 5 mils), the MMF vs. EMF plot becomes less

steep, allowing for changes in MMF to yield smaller changes in EMF. But the efficiency decreases with an increase in air gap. Figure 35 shows that the original 40 kVA example machine design with an air gap of 20 mils will reach 110 V at about 350 amp-turns, while that with an air gap of 50 mils will not reach 110 V until about 750 amp-turns.

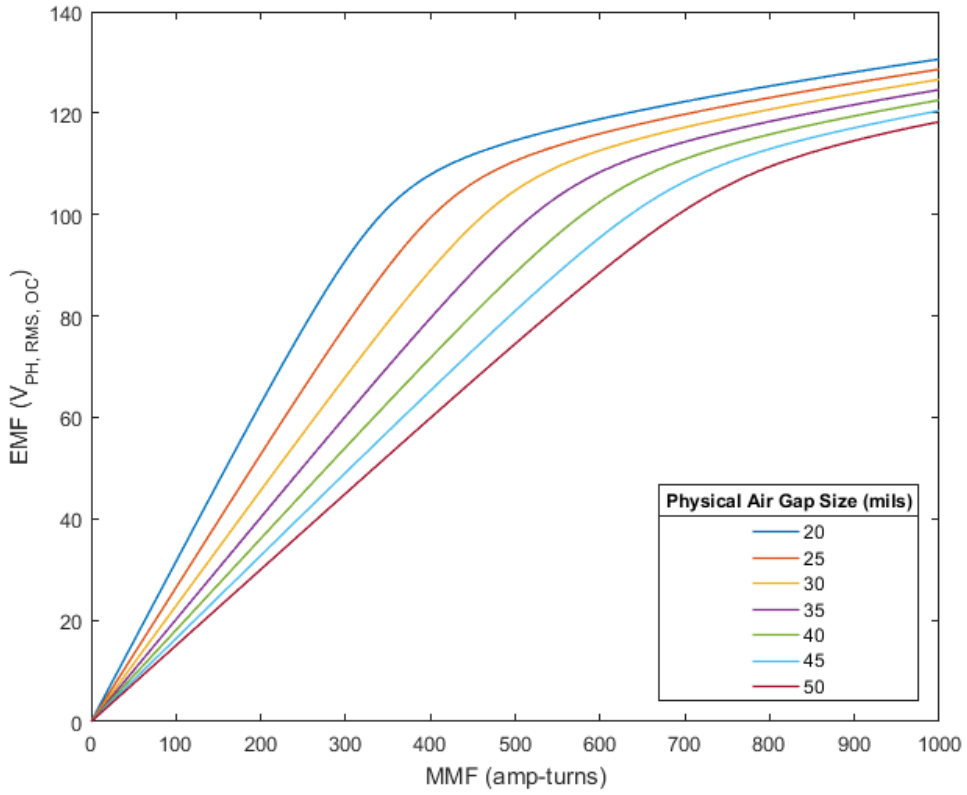

Figure 35: OC saturation plot for 40 kVA design, sweeping air gap

Direct-quadrature (dq) axis reactance parameters are now examined. Figure 36 shows the change in per-unit synchronous reactance as a function of sweeping the physical air gap from 20 – 50 mils. Plotted are the per-unit direct axis unsaturated synchronous reactance ($X_{d\,pu}$) and the per-unit quadrature axis unsaturated synchronous reactance ($X_{q\,pu}$). Both decrease as air gap size increases. At an air gap of 20 mils, the values of $X_{d\,pu}$ and $X_{q\,pu}$ are 1.643 Ω/phase and 1.065 Ω/phase, respectively. In

comparison, the $X_{d\,pu}$ and $X_{q\,pu}$ values of a similar tested 40 kVA generator from [19] are 1.66 Ω/phase and 0.735 Ω/phase, respectively.

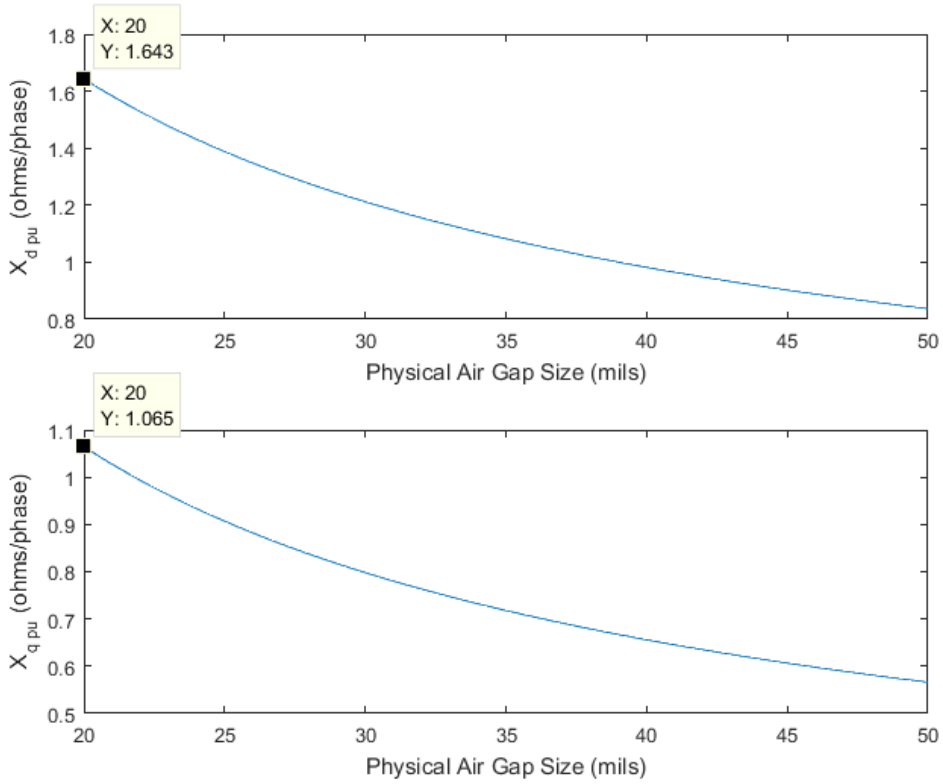

Figure 36: Per-unit unsaturated synchronous reactances for 40 kVA design

Figure 37 shows how the impedance changes while sweeping the air gap size and shear stress.

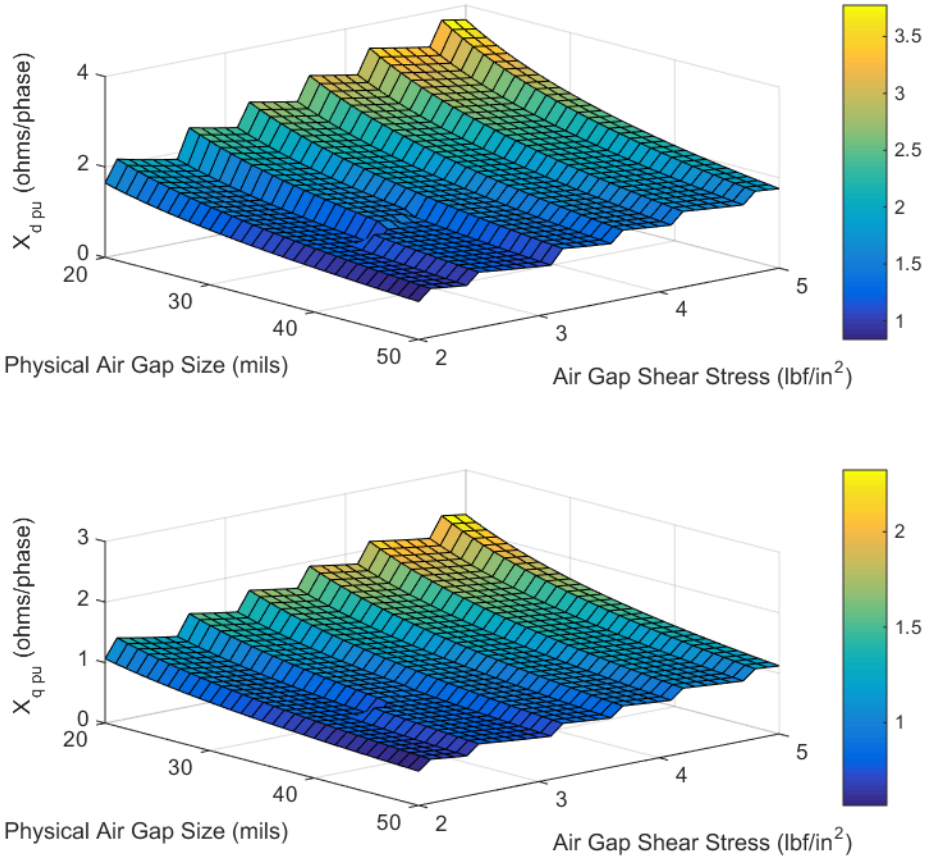

Figure 37: $X_{d\&q\ pu}$ for 40 kVA design vs. air gap size, shear stress

The effective number of phase turns, $N_{\varphi\ eff}$, and lost phase turns, $N_{\varphi\ lost\ eff}$, are now calculated:

$$N_{\varphi\ eff} = f_b \times N_{\varphi} = 0.814 \times 28 = 22.784 \tag{37}$$

$$N_{\varphi\ lost\ eff} = N_{\varphi} - N_{\varphi\ eff} = 28 - 22.784 = 5.216 \tag{38}$$

The generator effectively lost just over 5 coil turns due to winding configurations aimed at eliminating harmonics in the output voltage waveform.

The harmonic content for the 40 kVA design is now plotted: the magnitude of the total winding factor, k_w, is plotted for up to the 51st harmonic (Figure 38), and then zoomed in up to the 21st harmonic (Figure 39).

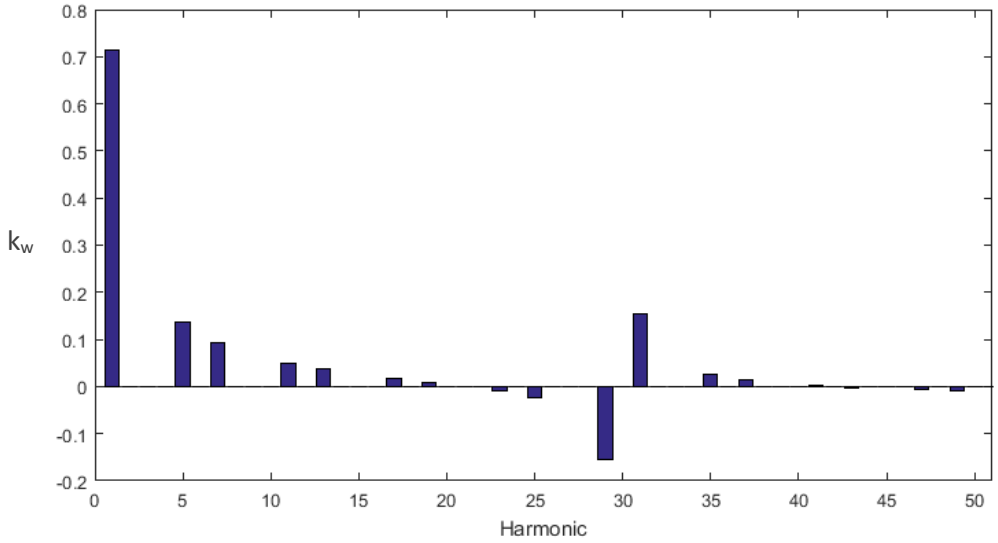

Figure 38: Through 51st harmonic for 40 kVA design

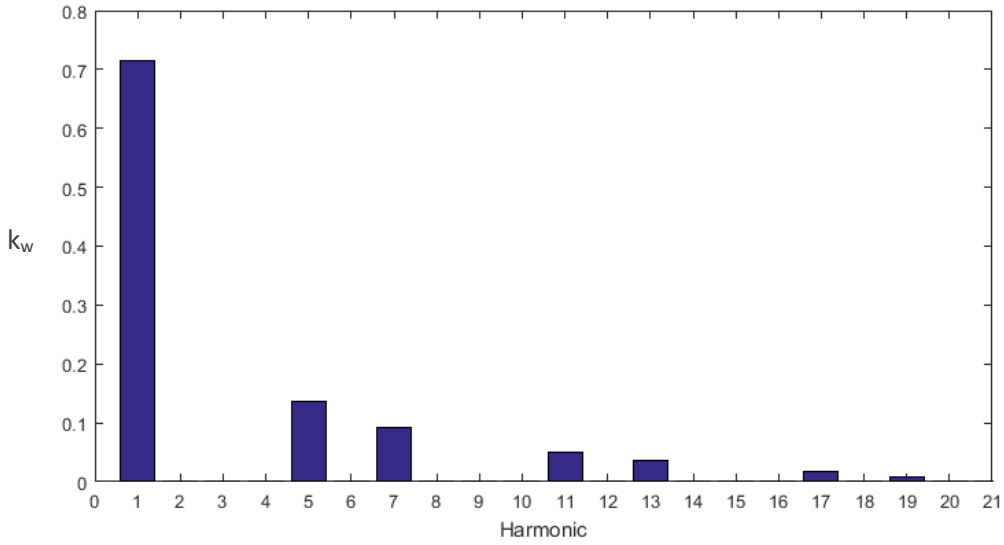

Figure 39: Through 21st harmonic for 40 kVA design

3.3: 250 kVA VSVF Example

A variable speed, variable frequency (VSVF) machine 250 kVA example is now investigated. Use of VSVF power generation "allows designers to discard the complex and difficult-to-maintain equipment necessary to convert variable-speed mechanical power produced by the engines to constant-frequency electrical power traditionally used by aircraft systems. By this way, variable-frequency power generation increases reliability of the whole system" [2]. This VSVF machine is to have a 2:1 speed ratio, ranging from 7500 rpm to 15,000 rpm. At all of the speeds within this range, minimum power (250 kVA) and voltage (235 V) must be provided. Table 4 lists the key inputs:

Table 4: 250 kVA design inputs

Parameter	**Value**	**Units**
Continuous Power Rating	250	kVA
Voltage	235	$V_{ph\ rms}$
Power Factor	0.85	
Overload	1.25	
Current Density	30	kA/in^2
Phases	3	
Wire type	copper	
Air Gap Size	20	mils
Air Gap Shear Stress	5	psi
Rotor Speed	7500	rpm
Max Rotor Speed	15,000	rpm
Length to Diameter Ratio	0.5 – 2.0 (sweep)	
Slot to Tooth Ratio	0.5 – 2.0 (sweep)	
Stack Factor	0.93	
Slots Skew	1	
Pole Embrace	0.75	
# Poles	6	
Maximum Tip Speed	650	fps
Rotor Steel Type	Hiperco-50	
Stator Steel Type	Hiperco-50	

Unknown inputs for this example are L/D ratio, S/T ratio, and air gap shear stress. An assumption for the shear stress in this example is 5 psi, a value on the higher end for aerospace generators. Such an assumption is used because, if a machine arising out of this example were to be produced today, there would likely be high cooling capabilities, allowing for higher TRV which is a result of higher shear stress. So the two remaining

unknowns, L/D ratio and S/T ratio, are both swept from 0.5 – 2.0 as inputs in this example.

Violations are first investigated. Figure 40 shows the tip speed as a function of L/D ratio and S/T ratio. In this example, the tip speed only changes with the L/D ratio. The highest tip speed (based off the highest envisioned rotor speed) does not exceed 650 fps, so there are no violations from the tip speed check.

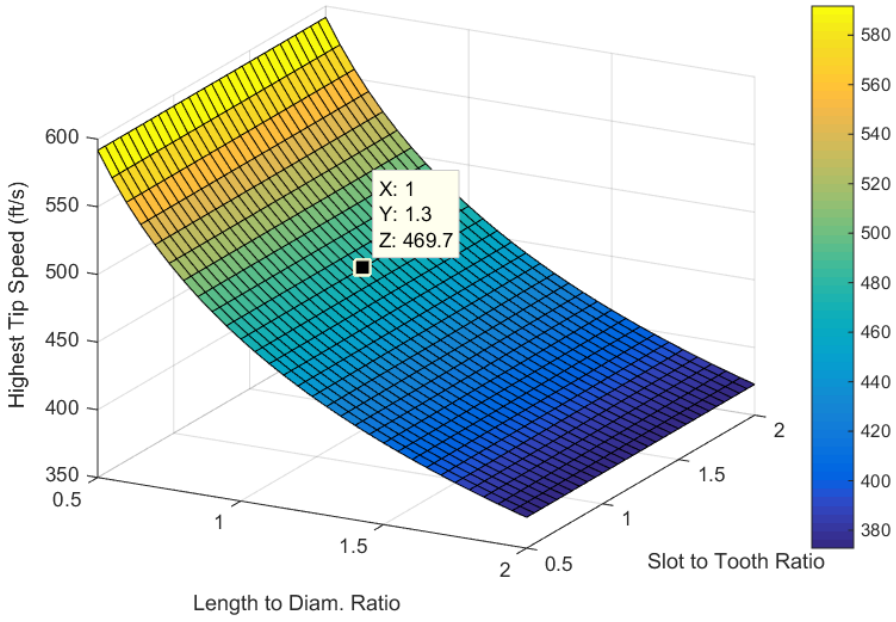

Figure 40: Tip speed plot for 250 kVA design

The tip speed only changes with L/D ratio because the tip speed is directly proportional to the rotor diameter (Figure 41). And with a given rotor volume (which is calculated independent of S/T ratio), the only factor that will affect the rotor diameter is the L/D ratio. The stack length is correspondingly calculated.

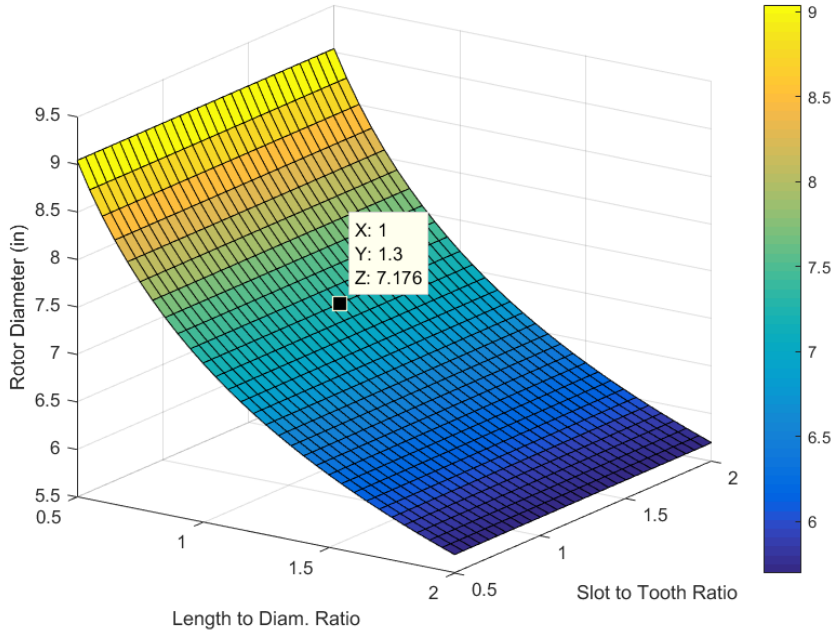

Figure 41: Rotor diameter plot for 250 kVA design

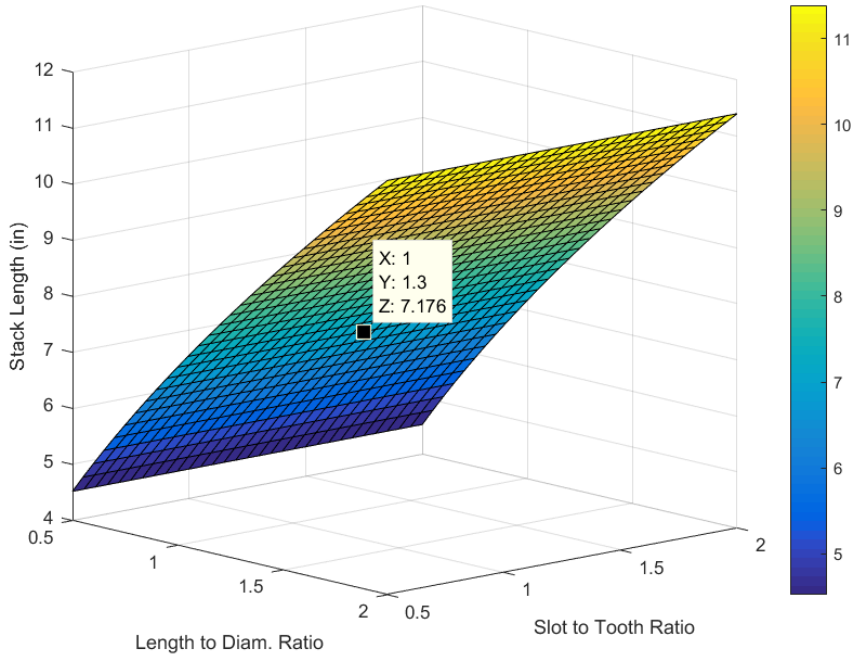

Figure 42: Stack length plot for 250 kVA design

The pitch ratio is 0.57, not the ideal 2/3.

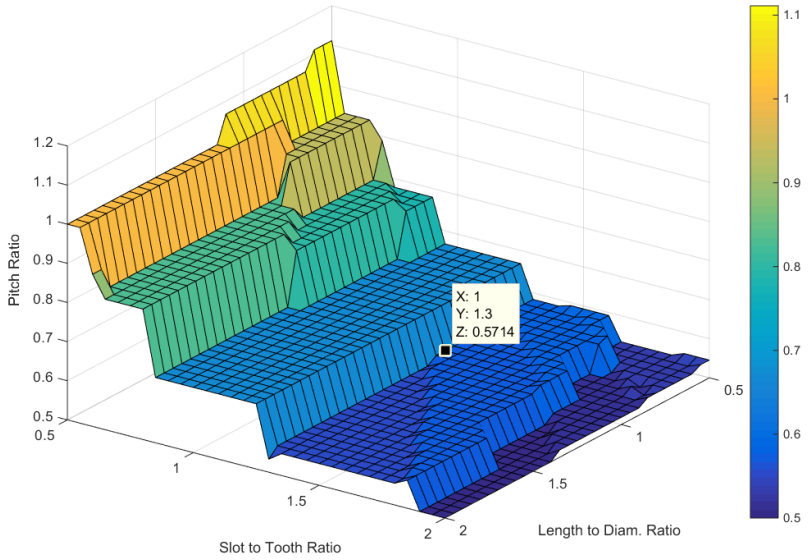

Figure 43: Pitch ratio plot for 250 kVA design

The calculated slot width meets the minimum slot width for nearly all of the design points, as shown in Figure 44 and Figure 45.

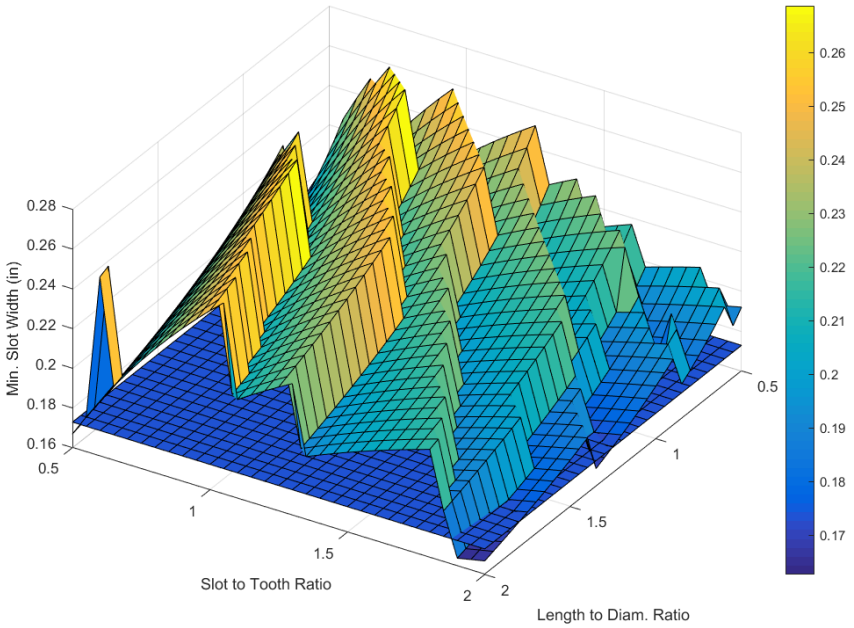

Figure 44: Slot width plot for 250 kVA design

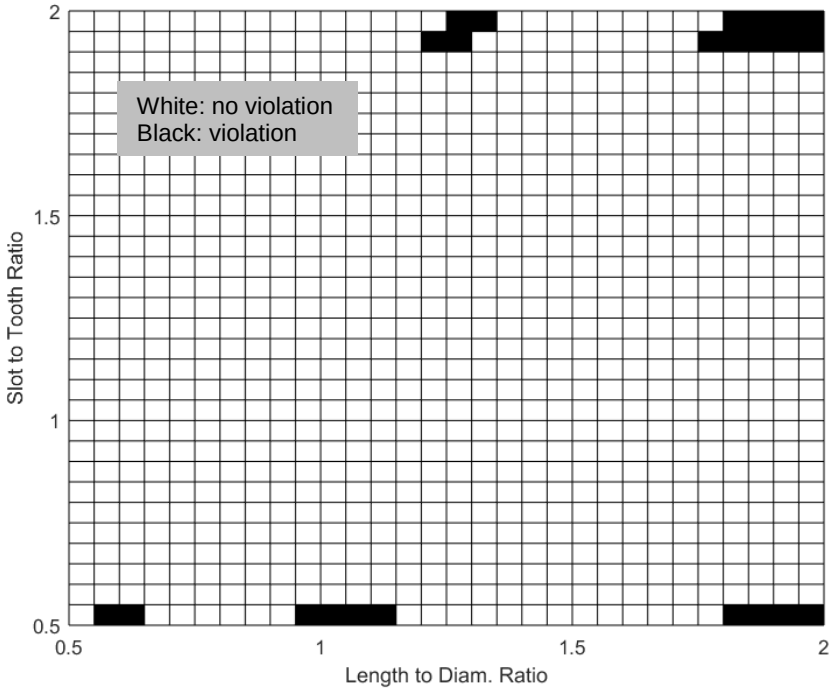

Figure 45: Violation check plot for 250 kVA design

To satisfy the goal of having the slots/pole/phase to be a whole number plus 1/2 (see Section 2.2.12), an L/D ratio of 1 and an S/T ratio of 1.3 were chosen to obtain 3.5 slots/pole/phase.

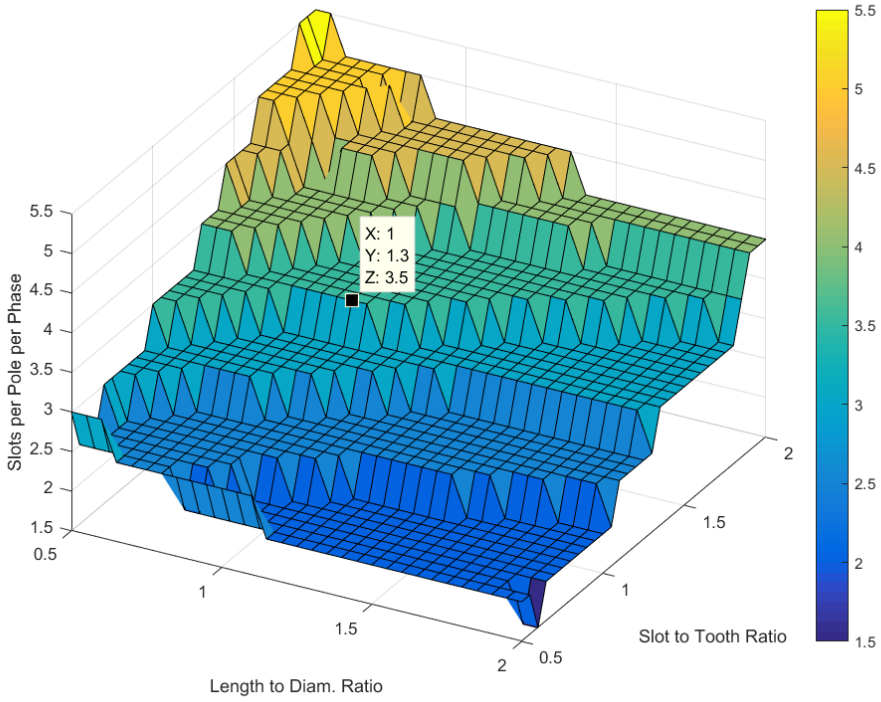

Figure 46: Slots per pole per phase plot for 250 kVA design

The total weight is calculated to be 219.7 lbs.

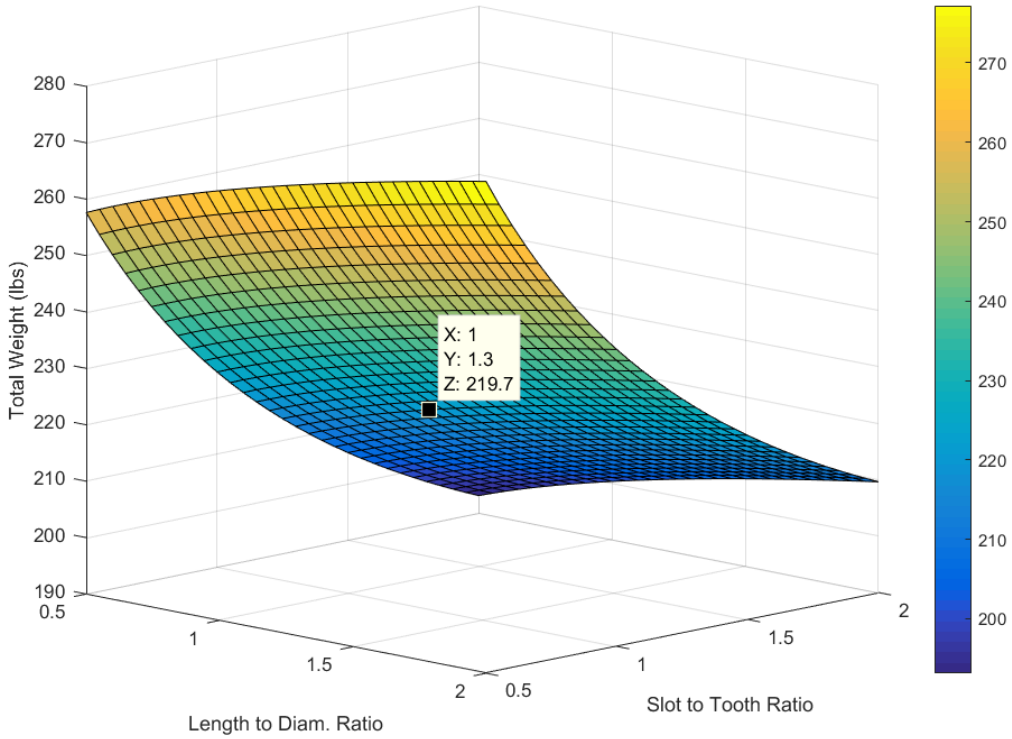

Figure 47: Weight plot for 250 kVA design

The air gap shear stress is now swept: 2, 3.5, and 5 psi, for the purposes of comparing their corresponding weight plots. Figure 48 shows that weight increases with decreased shear stress.

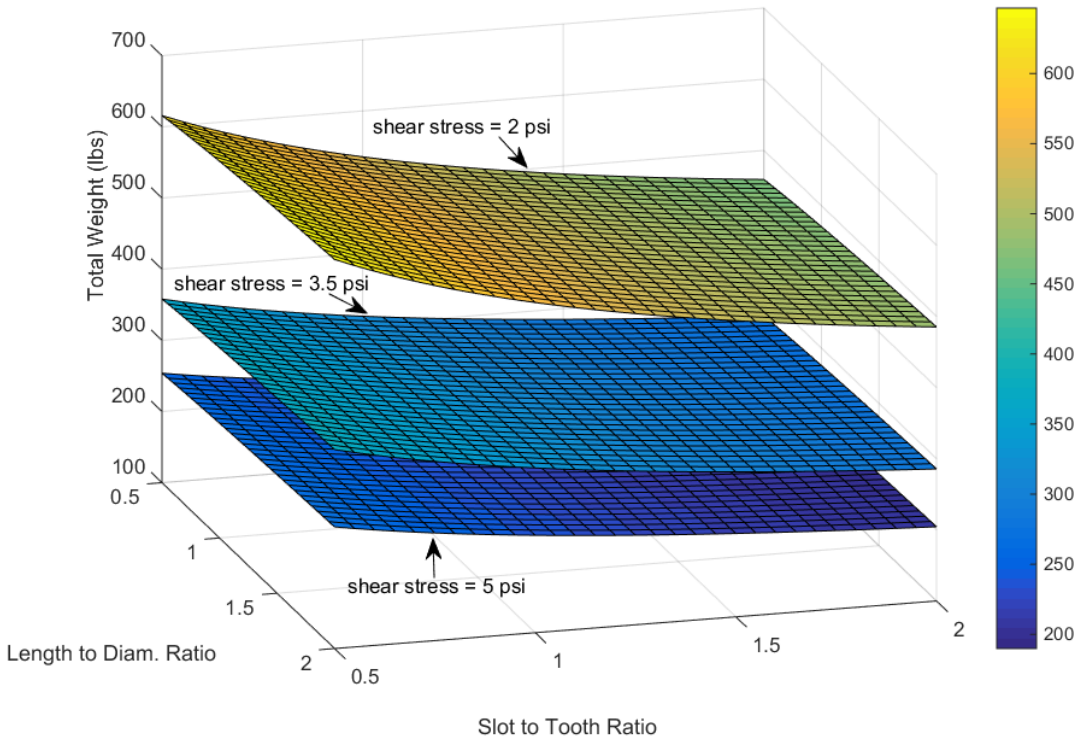

Figure 48: Weight plot for 250 kVA design, sweeping psi

For the chosen design point (x: L/D ratio = 1, y: S/T ratio = 1.3), the machine's open-circuit (OC) voltage characteristics are now simulated, as was done for the 40 kVA example. On the x-axis the MMF is swept from 0 – 1000 amp-turns (appropriate window for showing the amp-turns necessary on the rotor field to generate the intended OC voltage). In practice, this characterization test for a two-stage machine would have the input DC excitation current for the exciter generator on the x-axis, since the magnetic field strength cannot be measured while the machine is spinning. Shown in Figure 49 are the OC voltage curves for the machine at four speeds and corresponding frequencies, ranging from 7500 – 15,000 rpm (375 – 750 Hz). The output voltage curves rise with speed/frequency and magnetic flux, which increases with magnetic field strength. These two phenomena can be confirmed by Equation 4:

$$E = \sqrt{2}\pi f_b N_\varphi f \Phi \tag{4}$$

The steel in the machine starts to saturate at an input magnetic field strength of about 500 amp-turns, which can be seen by a bend in the output voltage. As explained in Section 2.2.14, any machine operation past this point is inefficient because there are diminishing returns: the back EMF increases by less than before as the input MMF increases beyond about 500 amp-turns. These diminishing returns are due to core losses within the steel. For the 7500 rpm operating point plot, the saturation voltage is about 235 V as expected.

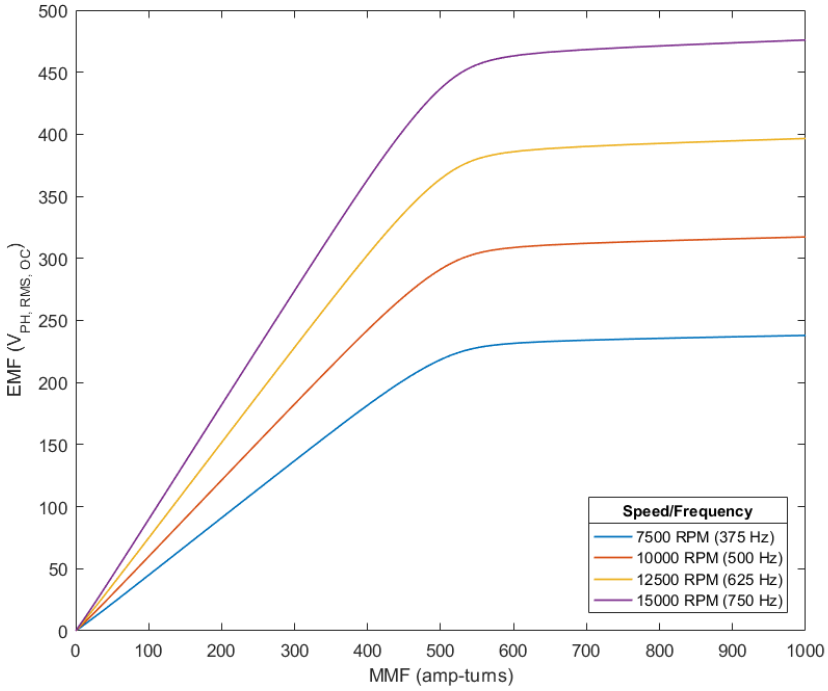

Figure 49: OC saturation plot for 250 kVA design

The OC voltage plot is now examined while sweeping the air gap for the chosen design point. As the air gap size is swept from 20 – 50 mil, the MMF vs. EMF plot becomes less steep, allowing for changes in MMF to yield smaller changes in EMF. But the efficiency decreases with an increase in air gap.

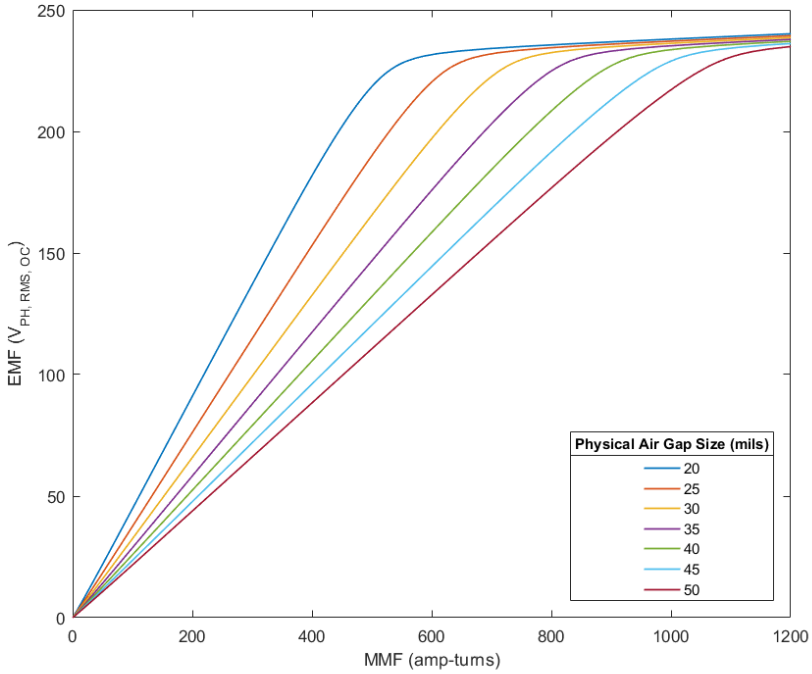

Figure 50: OC saturation plot for 250 kVA design, sweeping air gap

Direct-quadrature (dq) axis reactance parameters are now examined. Figure 51 shows the change in per-unit synchronous reactance as a function of sweeping the physical air gap from 20 – 50 mils. Plotted are the per-unit direct axis unsaturated synchronous reactance ($X_{d\,pu}$) and the per-unit quadrature axis unsaturated synchronous reactance ($X_{q\,pu}$). Both decrease as air gap size increases. At an air gap of 20 mils, the values of $X_{d\,pu}$ and $X_{q\,pu}$ are 3.033 Ω/phase and 2.257 Ω/phase, respectively.

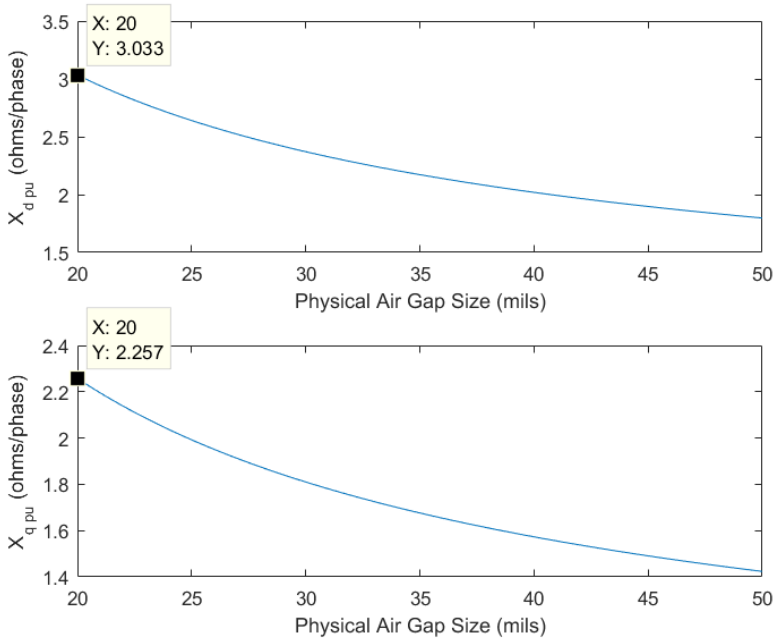

Figure 51: Per-unit unsaturated synchronous reactances for 250 kVA design

Figure 52 shows how the impedance changes while sweeping the air gap size and shear stress.

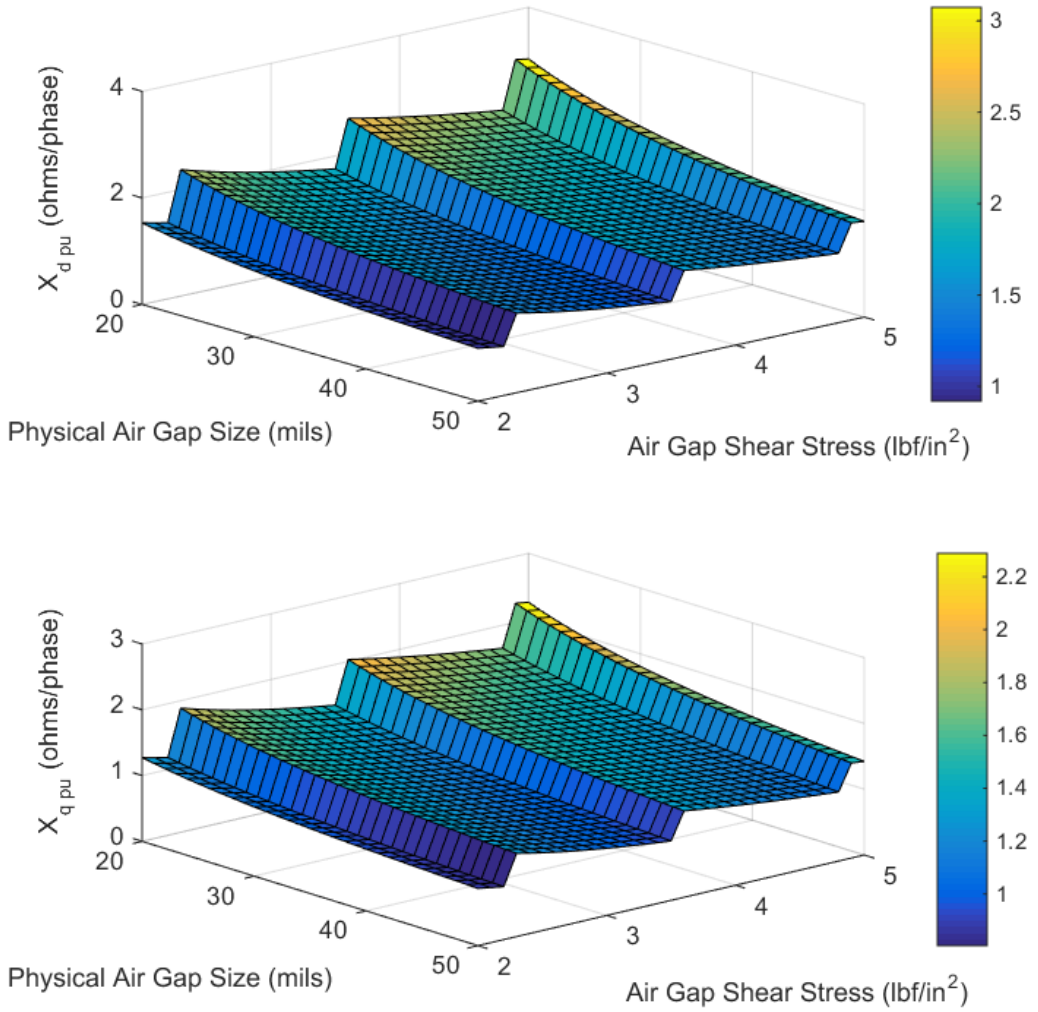

Figure 52: $X_{d\&q\ pu}$ for 50 kVA design vs. air gap size, shear stress

The effective number of phase turns, $N_{\varphi\ eff}$, and lost phase turns, $N_{\varphi\ lost\ eff}$, are now calculated:

$$N_{\varphi\ eff} = f_b \times N_{\varphi} = 0.812 \times 15 = 12.183 \tag{39}$$

$$N_{\varphi\ lost\ eff} = N_{\varphi} - N_{\varphi\ eff} = 2.817 \tag{40}$$

The generator effectively lost just under 3 turns due to winding configurations aimed at eliminating harmonics in the output voltage waveform.

The harmonic content for the 250 kVA design is now plotted: total winding factor, k_w, is plotted for up to the 51st harmonic (Figure 53), and then zoomed in up to the 21st harmonic (Figure 54). Since the pitch ratio of the design is not 2/3, the 3rd, 9th, and 15th harmonics are not eliminated, though the 7th is eliminated.

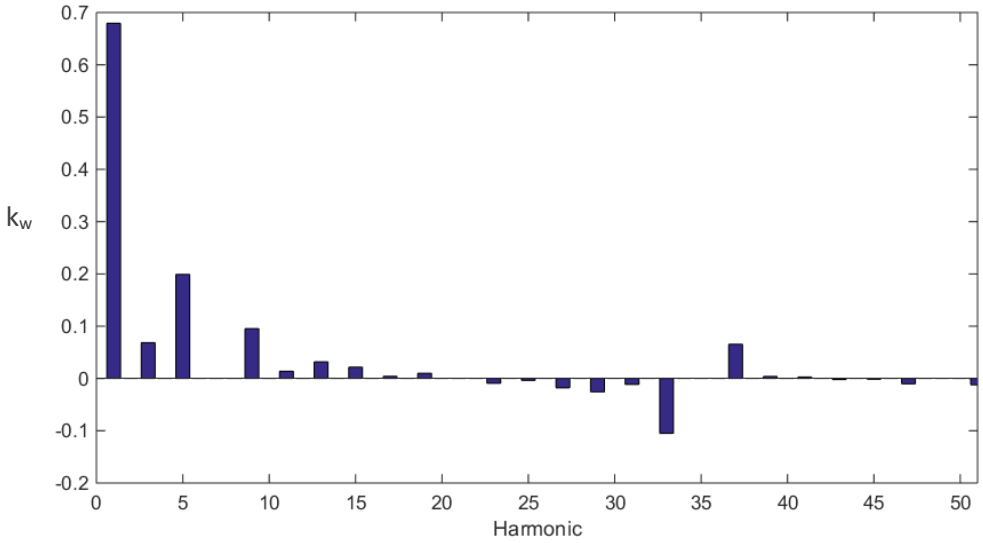

Figure 53: Through 51st harmonic for 250 kVA design

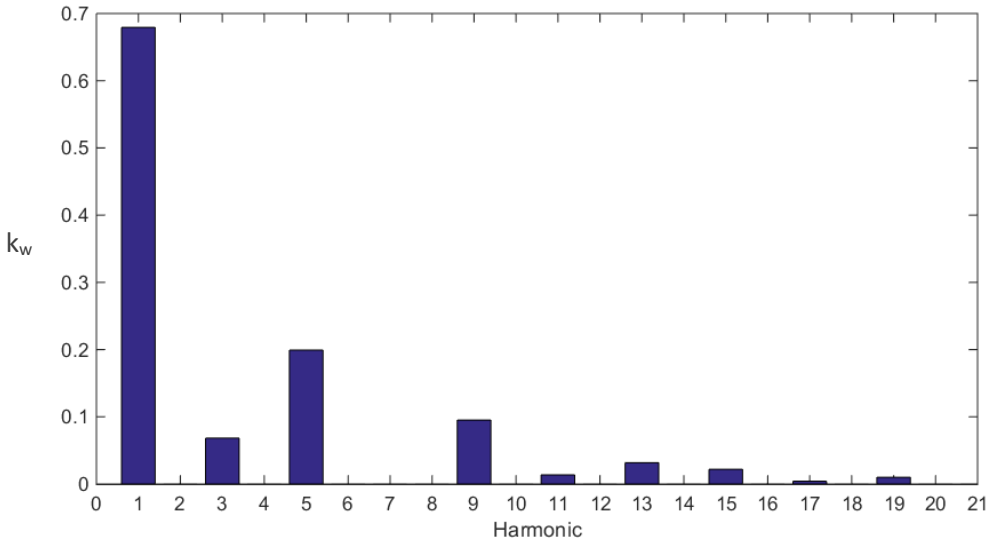

Figure 54: Through 21st harmonic for 250 kVA design

For comparison purposes, the harmonics content of a design point for this 250 kVA example with 2/3 pitch (L/D ratio = 1 and S/T ratio = 1) is plotted: the magnitude of the total winding factor, k_w, is plotted for up to the 51st harmonic (Figure 55), and then zoomed in up to the 21st harmonic (Figure 56). Since the pitch ratio of the design is 2/3, the 3rd, 9th, and 15th harmonics are eliminated, though the 7th harmonic does appear.

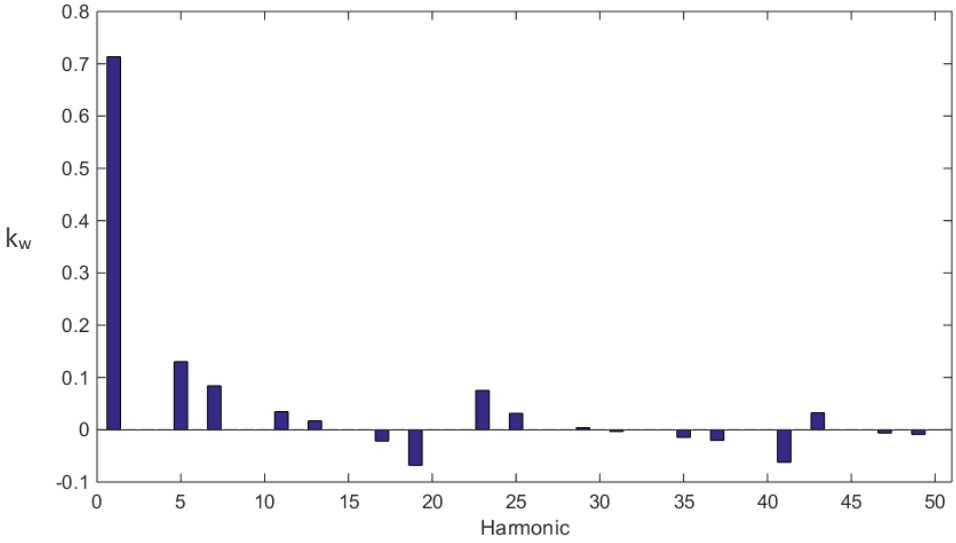

Figure 55: Through 51st harmonic for updated 250 kVA design (2/3 pitch)

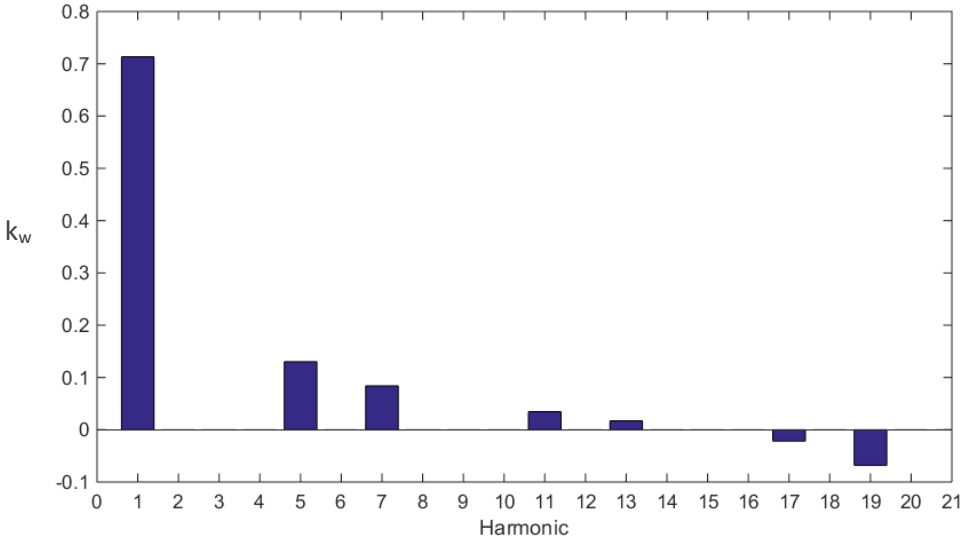

Figure 56: Through 21st harmonic for updated 250 kVA design (2/3 pitch)

Chapter 4: Conclusions and Recommendations

This generator sizing tool sizes 100s to 1000s + of machines quickly, within seconds (depending on the speed of the computer). It is a good tool for analyzing design trends for a given conceptual machine (such as for the 250 kVA example). It provides initial sizing estimates for preliminary machine design. The confidence in the tool is strongest for the 40 kVA generator example in which many aspects are known, including the input parameters, because the outputs of the model can be compared to the physical generator. Uncertainty increases in branching out from this generator design point.

Unless specifically instructed otherwise, the default action of this generator sizing tool is to size for what is minimally necessary. For example, the 40 kVA generator example's actual shear stress was 2.88 psi, but was chosen to be 2 psi in the program to yield similar dimensions between the conceptual and physical generators. If the shear stress had been 2.88 psi in the program, the volume would have been smaller than the actual volume. So this generator, as likely with many generators, appears to be slightly overdesigned, in that more than the minimum volume was used. A reason for doing so may be to ensure thermal stability.

The rated generator voltage, as shown in Figure 57, is generally chosen to be on the OC curve at the point after which the voltage begins to saturate. The point (seen in red) at which the voltage begins to saturate, however, is a more efficient operating point since saturation has not yet occurred. This point, though, is at a lower voltage than the original rated voltage. Designing for the rated voltage to be at the initial point of saturation would require an increase in generator size and weight; doing so may

compromise the benefit of a more efficient operating point. Thus consideration of these points should be taken in designing for the rated voltage operating point.

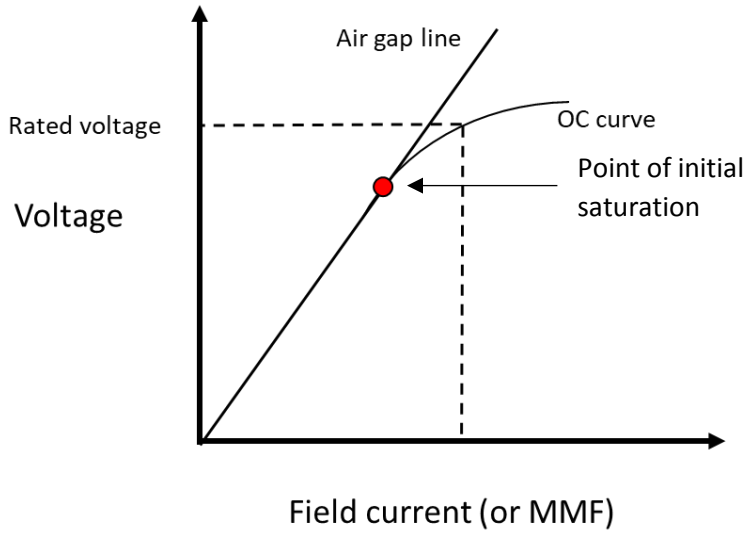

Figure 57: Plot of open-circuit test (initial saturation)

Program enhancements that can be done are:

- Improve weight calculations, power loss, and efficiency calculations.
- Improve geometrical configurations, especially on the rotor when there is a high number of poles.
- In addition to the feasibility checks of L/D ratio, tip speed, and slot width, perform additional feasibility checks: ensure the number of turns on the rotor for producing the field is not too high, and ensure that the shaft is of appropriate diameter to handle the machine torque.
- Calculate transient and subtransient reactances.
- Calculate thermal aspects: rate of heat transfer from system into environment, changes in internal energy, exergy destruction rate, and entropy generation rate.
- Improve insulation size estimates based off rated voltage.

- Size for the exciter machine: similar calculations to sizing for the main machine are expected to be performed if the exciter machine is sized.
- Allow for use of more than 2 conductors/slot (gives potential for higher voltage).

Project improvements that can be done are:

- Semi-validate program with lab results from sample 40 kVA generators. Caution should be exercised in doing this however, as the sizing tool currently only models the main machine.
- Use program results as reference for Finite Element Analysis (FEA). Compare direct-quadrature (dq) axis reactance parameters, losses information, and OC voltage curves. Programs for doing this include Maxwell and Motorsolve.
- Feed output dq parameters of model in dq simulation program to analyze steady-state, transient and subtransient behavior of generator.
- Perform statistical sensitivity analysis on design considerations to determine higher payoff design choices.
- Perform multidisciplinary optimization analysis: future aircraft will require high amounts of reliable electrical power. Because the generator affects many other components on an aircraft, there is a need for an integrated system analysis, where the generator is designed while considering the effect each design aspect has on both the generator and other systems, in accordance with industry standards. In doing so, any mistakes should be corrected early on to avoid run-over costs and delays.

References

[1] S. Iden, K. J. Yost, M. R. von Spakovksy, D. L. Allison and D. D. Gross, "Conceptual Design Methods for New Aircraft Generators," in *AIAA Aviation Forum*, Denver, 2017.

[2] J. A. Rosero, J. A. Ortega, E. Aldabas and L. Romeral, "Moving Towards a More Electric Aircraft," *IEEE A&E Systems Magazine*, pp. 3-9, March 2007.

[3] "Chapter 12: Hydraulic and Pneumatic Power Systems," Federal Aviation Administration, Washington, DC, 2014.

[4] C. R. Nave, "HyperPhysics," Georgia State University, 2016. [Online]. Available: http://hyperphysics.phy-astr.gsu.edu/hbase/emcon.html#emcon. [Accessed 1 March 2018].

[5] P. C. Sen, Principles of Electric Machines and Power Electronics, Hoboken, NJ: John Wiley & Sons, 2014.

[6] J. H. Kuhlmann, Design of Electrical Apparatus, 2nd ed., New York: John Wiley and Sons, 1940.

[7] A. von Meier, Electric Power Systems: A Conceptual Introduction, Hoboken, New Jersey: John Wiley & Sons, Inc., 2006.

[8] J. E. Rucker, "Design and analysis of a permanent magnet generator for naval applications," Massachusetts Institute of Technology, Cambridge, MA, 2005.

[9] A. E. Fitzgerald, C. Kingsley, Jr. and S. D. Umans, Electric Machinery, Sixth ed., New York: McGraw-Hill, 2003.

[10] N. Levin, S. Orlova, V. Pugachov, B. Ose-Zala and E. Jakobsons, "Methods to Reduce the Cogging Torque in Permanent Magnet Synchronous Machines," *ELEKTRONIKA IR ELEKTROTECHNIKA*, vol. 19, no. 1, 2013.

[11] W. L. Soong, "Sizing of Electrical Machines," 26 September 2008. [Online]. Available: http://www.eleceng.adelaide.edu.au/research/power/pebn/pebn009%20sizing%20of%20electrical%20machines.pdf. [Accessed 2 March 2018].

[12] V. Rallabandi, N. Taran, D. M. Ionel and J. F. Eastham, "Coreless multidisc axial flux PM machine with carbon nanotube windings," in *2016 IEEE Conference on Electromagnetic Field Computation (CEFC)*, Miami, FL, 2016.

[13] T. E. Miller and D. A. Staton, SPEED's Electric Machine Design, Lulu Publishing, 2013.

[14] "Why is flyback air gap needed for energy storage?," StackExchange, 2013. [Online]. Available: https://electronics.stackexchange.com/questions/77797/why-is-flyback-air-gap-needed-for-energy-storage. [Accessed 5 May 2018].

[15] T. A. Lipo, Introduction to AC Machine Design, University of Wisconsin: Wisconsin Power Electronics Research Center, 2004.

[16] A. Knight, "TESTS TO FIND CIRCUIT PARAMETERS," University of Calgary, [Online]. Available: http://people.ucalgary.ca/~aknigh/electrical_machines/synchronous/s_tests.html. [Accessed 9 April 2018].

[17] T. A. Loehlein, "Calculating generator reactances," 2006. [Online]. Available: https://power.cummins.com/sites/default/files/literature/technicalpapers/PT-6008-GeneratorReactances-en.pdf. [Accessed 13 April 2018].

[18] R. Sasaki, M. Wada and O. Sakamoto, "Weight and Characteristics of Aircraft AC Generators Abstract," *Aeronautical and Space Sciences Japan*, vol. 27, no. 305, pp. 296-300, 1979.

[19] Airlines Electronic Engineering Committee, "Guidance for Aircraft Electrical Power Utilization and Transient Protection," Aeronautical Radio, Annapolis, MD, 1989.